Metamaterial Filters on LCP Substrate Using MEMS Technology

by

Jonathan Tyler Richard

A thesis submitted to the Graduate Faculty of
Auburn University
in partial fulfillment of the
requirements for the Degree of
Master of Science in Electrical Engineering

Auburn, Alabama
December 12, 2011

Keywords: Metamaterials, LCP, MEMS, Filter

Approved by

Robert Dean, Chair, Assistant Professor of Electrical and Computer Engineering
Stuart Wentworth, Associate Professor of Electrical and Computer Engineering
Lloyd Riggs, Professor of Electrical and Computer Engineering

Abstract

Metamaterials have a wide range of potential uses in areas such as optics, transmission lines, and RF design. The simplest metamaterial structures are Split-Ring Resonators (SRR) and Complementary Split-Ring Resonators (CSRR). Through the combination of various forms of these structures, different applications can be achieved. An in depth investigation was performed on a metamaterials transmission line that was realized through micromachining a Liquid Crystal Polymer (LCP) substrate. LCP was chosen because it possesses useful RF properties and can be easily micromachined. This transmission line consisted of several CSRRs in series, which performed as a high-order, high-frequency, band-pass filter. This structure is unique to most metamaterial structures because LCP is a flexible substrate. It was observed that the resonant frequency of the filter did not change when the LCP transmission line was flexed over various radii of curvature. Extrapolating these methods to the development of metamaterial 3D RF invisibility cloaks that are easily manufactured and mountable onto an object could prove useful.

Acknowledgements

The author would like to thank the following:

- his advisor, Dr. Robert Dean, for guidance and fabrication assistance
- his committee members Dr. Lloyd Riggs and Dr. Stuart Wentworth
- Dr. Hamilton for simulation guidance
- Dr. Charles Ellis for help in the fabrication lab and fabrication knowledge
- Joe Haggarty for aiding in copper etching
- Byron Caudle for help testing with the network analyzer

Table of Contents

List of Figures

List of Tables

1. Introduction

Metamaterials are man-made structures that are relatively new to the scientific world. These structures exhibit behaviors that are not commonly found in nature [11]. Specifically, they exhibit negative permittivity and permeability over small frequency ranges [26]. This can result in a backward propagation of traveling waves. Due to these properties, several applications can arise.

Metamaterials can be useful in various areas in the RF and optical world [12-14]. The most notorious area is for invisibility cloaks [15-16]. This area is still being heavily researched. Another area that metamaterials can prove useful is in transmission line applications. This application includes filters, power dividers, and sensors [29-33]. Much of the research is being performed on rigid substrates. The goal of this thesis was to prove that metamaterial structures do not change resonant frequency when placed onto a flexible substrate while being flexed.

Metamaterial filters were constructed on LCP. Then they were shown to not change resonance frequency while being contorted at extreme bends. Through extrapolation, metamaterial 3D cloaks could be constructed on LCP and not change resonance frequency while contorted. This would prove useful for a real-world 3D invisibility cloak [19-20, 31, 34].

2. Literature Review

In this chapter, types of substrates, the basic concepts of metamaterials, flexible metamaterials, and fabrication techniques are be discussed. The most common substrates used are rigid, such as Rogers R0310. Next, basic structures of metamaterials known as SRRs (Split Ring Resonators) and CSRRs (Complementary Split Ring Resonators) are discussed. This is followed by an introduction to flexible metamaterials and common flexible substrates. Two of these flexible substrates are Liquid Crystal Polymer (LCP) and Polyimide. Finally, common fabrication techniques will be overviewed.

2.1. Substrates

Metamaterial structures are designed for higher frequency applications. The frequencies can range from low GHz up to THz. With such a high frequency, special RF compatible substrates must be used. The more common substrate is usually rigid since rigid substrate fabrication techniques have been perfected for decades. However, any RF substrate will essentially work. Below are several types of substrates commonly used in conjunction with metamaterials.

2.1.1. Rogers

Rogers is a corporation that fabricates high frequency laminates [21]. Rogers R03010 is used in multiple applications for metamaterials because of its high frequency

reliability [1-2]. Rogers board has a dielectric constant of 10.2 and comes in varying heights from a manufacturer. These heights are much thicker than their flexible counterparts.

2.1.2. LCP

LCP is less common among the metamaterial world, but it has some advantages over Rogers laminates. The main advantage is flexibility while a minor advantage is resistance to moisture absorption [28]. Flexibility proves useful in certain scenarios such as a 3-D invisibility cloak. When purchased from a manufacturer, LCP already has either one or both sides laminated with copper foil and has a relative permittivity of 3.1 [10]. Wet and dry processes to etch through LCP are also known and can be advantageous to use in certain designs [4-5]. Etching copper on LCP can be treated similarly to a rigid substrate with feature sizes around 100 μm or smaller if a backing wafer is used.

2.1.3. Polyimide

A Polyimide is a polymer composed of imide monomers. Polyimides are less common among the metamaterial world along with LCP. Polyimides are also commercially available but cost significantly more than LCP. The distinct advantage that polyimides have over LCP is that polyimdes operate reliably in terahertz frequencies [8, 34]. Additionally, Polyimides can be deposited onto a substrate [34]. Similar to LCP, some polyimides can also be dry etched.

2.2. Metamaterial Structures

There are two basic metamaterial structures. They are the Split-Ring Resonator (SRR) and the Complementary Split-Ring Resonator (CSRR). There are derivations of each structure, such as edge coupled (EC-SRR) or broadside coupled (BC-SRR) [17]. Each of these structures can be represented by equivalent circuit models and are shown in Figures 2.1 and 2.2 [22-25]. In the figures, L and C represent the per-unit inductance and capacitance of the line. Cg is the gap capacitance across the transmission line. Cc and Lc are the capacitance and inductance of the rings for a CSRR. Ls' and Cs' represent the mutual inductance and capacitance of a SRR. It has been observed that magnetic coupling is dominant in SRRs while electrical coupling is dominant in CSRRs. The structures must also be relatively small compared to the frequency of operation [17].

It is important to note that the circuits shown in Figures 2.1 and 2.2 were created based off of empirical data and equations for calculating the transfer function have been derived in equations 2.9-2.14. The values can be calculated using equations 2.1-2.5 by having three equations and three unkowns [6 pp 124, 168, 171]. Figure 2.3 shows a visualization of a CSRR cell where the brown represents the ground plane and yellow represents the transmission line. The inverse structure would be a SRR cell. It is possible to extract parameters from either electromagnetic simulations or measured data [24]. Calculating the parameters from equations is also possible but the equations are based off of empirical data for a simple SRR as shown in equations 2.6-2.8 of [6 pp 108-109].

$$f_H = \frac{1}{(2\pi\sqrt{L_C C_C})}$$ Eqn. 2.1

$$f_z = \frac{1}{(2\pi\sqrt{L_C(C + C_C)})}$$ Eqn. 2.2

$$Z_S(\omega_{\pi/2}) = -Z_P(\omega_{\pi/2})$$ Eqn. 2.3

$$Z_S(\omega) = j\omega\mu_{eff}$$ Eqn. 2.4

$$Y_p(\omega) = j\omega\varepsilon_{eff}$$ Eqn. 2.5

$$\frac{L}{u0} = \frac{pi^3}{4 * c^2}\int_0^\infty \frac{1}{k^2} * (\, bB(kb) - aB(ka)\,)^2 dk$$ Eqn. 2.6

Where C = line width, r = radius of circle, a = r – c/2, b = r + c/2, k = a/b, and

B(x) = $S_0(x)$ $J_1(x)$ - $S_0(x)$ $J_1(x)$, where S_n and J_n are nth order Struve and Bessel functions.

$$\frac{Cpul}{\varepsilon 0} = \frac{1}{2} * \varepsilon_e \left\{2 * \frac{c}{t} + 1.393 + .667 * \ln\left(2 * \frac{c}{t} + 1.444\right)\right\}$$ Eqn. 2.7

$$\varepsilon_e = \frac{\varepsilon + \varepsilon 0}{2 * \varepsilon 0} + \frac{\varepsilon - \varepsilon 0}{2\varepsilon 0}\left(1 + \frac{6t}{c}\right)^{-1}$$ Eqn. 2.8

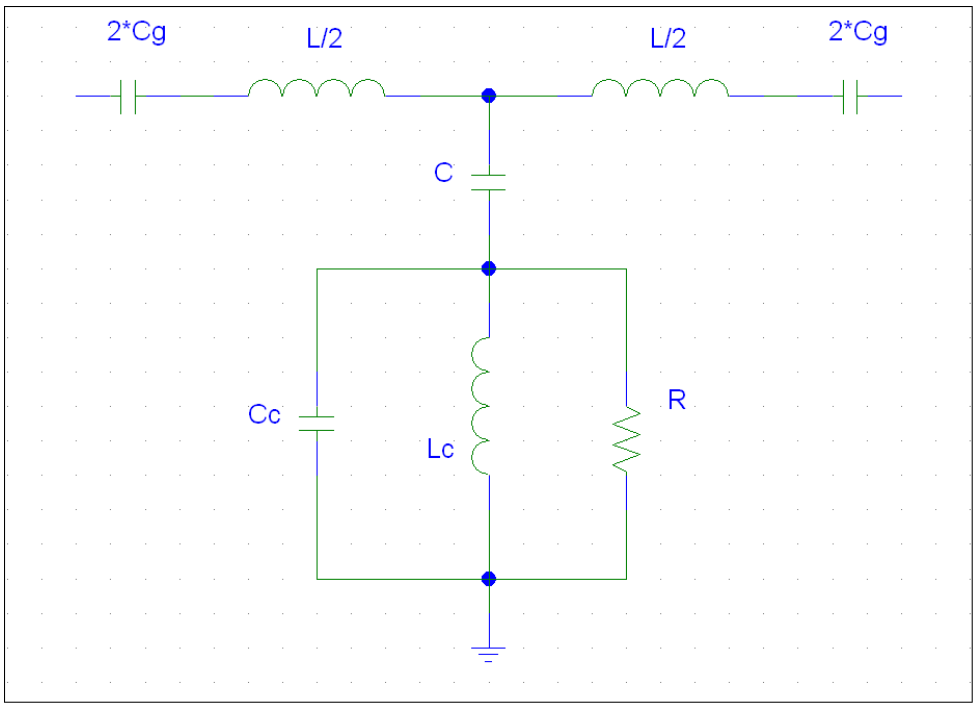

Figure 2.1: CSRR equivalent circuit model

$$Z_s = \frac{L}{4 * C_G}$$ Eqn. 2.9

$$Z_p = \frac{1}{(\frac{C}{L_C} - \omega^2 C C_c + \frac{j\omega c}{r})}$$ Eqn. 2.10

$$Z = Z_s * \frac{Z_p}{Z_s}$$ Eqn. 2.11

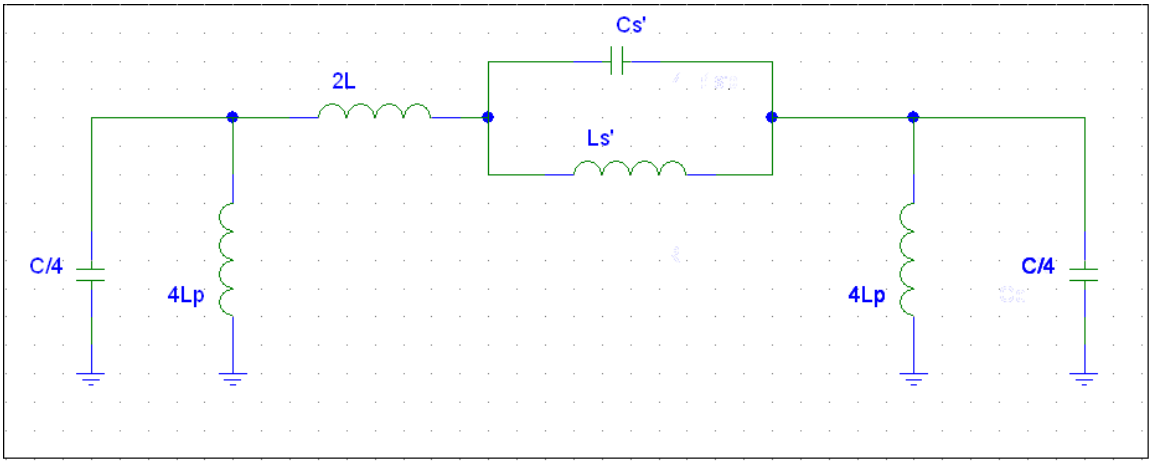

Figure 2.2: SRR equivalent circuit model

$$Z_s = \frac{-\omega^2 * 8L * L_s}{1-\omega^2 L_s C_s} \quad \text{Eqn. 2.12}$$

$$Z_p = \frac{j\omega 4L}{1-\omega^2 LC} \quad \text{Eqn. 2.13}$$

$$Z = Z_p^2 * Z_s \quad \text{Eqn. 2.14}$$

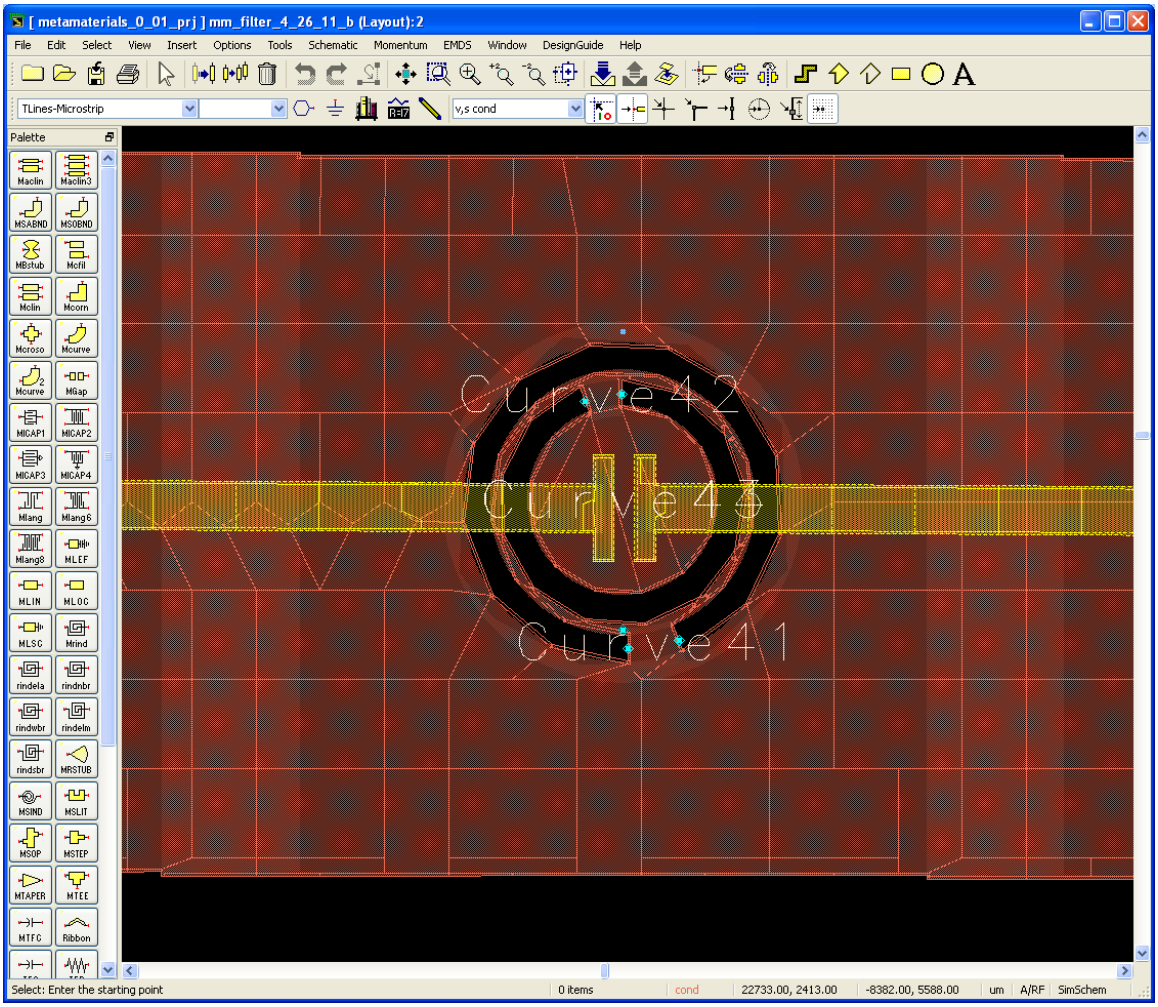

Figure 2.3 : CSRR Visuallization

The effective permeability, μ_{eff}, and effective permittivity, ε_{eff}, can also be found through calculation. Equations have to be made for each specific case. For a composite right/left handed transmission line, equations 2.15 and 2.16 from [6 pp 126] yield the permittivity and permeability.

$$\varepsilon_{eff} = \frac{C_R}{l} - \frac{1}{\omega^2 L_L l} \qquad \text{Eqn. 2.15}$$

$$\mu_{eff} = \frac{L_R}{l} - \frac{1}{\omega^2 C_L l} \qquad \text{Eqn. 2.16}$$

Where L_L and C_L are the dual transmission line inductance and capacitance and L_R and C_R are the per-section inductance and capacitance of the host line.

2.3. Flexible Metamaterials

Flexible metamaterials have been introduced onto polyimide and kapton layers. The use of standard photolithography with a backing wafer could be used in some cases in order to obtain smaller feature sizes of several microns [8,9]. In other cases, polyimide and any metals needed for fabrication were deposited [8, 34].

2.4. Fabrication Techniques

The vast majority of published metamaterial oriented papers use standard photolithography processes. Only a few differences occur. One of these differences is either buying prebuilt substrates [9] or deposition of a substrate onto a silicon wafer [8]. Another difference was the use of a backing wafer to obtain significantly smaller feature sizes on a flexible substrate [8, 34].

2.5 Bloch Impedance

Metamaterial transmission lines consist of multiple resonant structures. Each structure can be defined as a T-circuit of series and shunt impedances. From analysis of multiple structures, a characteristic (or Bloch) impedance can be defined. Ideally, this impedance should be matched to 50Ω for the desired frequency. From the given values and equations in [7], the Bloch impedance was 50Ω for only one value but jumped up to 350Ω as well as shown in Figure 2.4. While there is definitely some change of impedance caused by removal of metal in the ground plane from a metamaterial structure,

Bloch impedance does not properly solve for the impedance. There are more detailed plots of Bloch impedance as shown in [1] and [6 pp 178] but the impedance is only 50 Ω for a small frequency band.

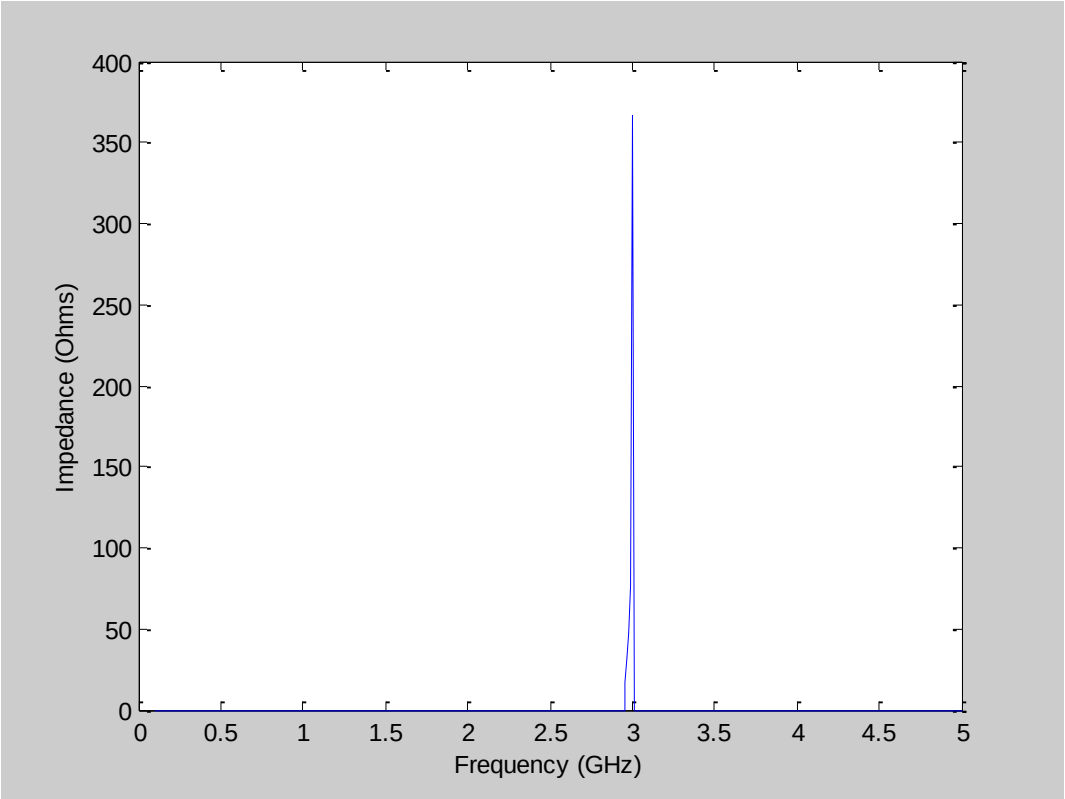

Figure 2.4: Bloch Impedance vs. Frequency

2.6. Metamaterial Filters

One of the main areas being researched is tunable metamaterial filters [22,27]. One approach involves a cascaded right-handed and left-handed transmission line [22]. The unique part that makes it variable is not the metamaterial portion. Varactor diodes are placed into the right-handed transmission line. By varying the voltage across the diodes, that part of the transmission line will change resonance frequency and provide a narrow passband filter.

3. Equipment and Software

In this chapter, laboratory equipment and software is discussed. Software will be presented in the order in which it was needed in design. Equipment will be presented in the order it was used in fabrication.

3.1. Simulation and Data Analysis

The following programs were used to simulate a design, layout a design, or plot that has been gathered.

3.1.1. Agilent ADS 2009

Agilent ADS, a commercially available electromagnetic simulation software package, proved to be a useful tool. One part of ADS that was particularly useful was LineCalc. LineCalc provided a calculator that could calculate impedance based off of line width, substrate thickness, relative permittivity of substrate, copper thickness, and frequency. This was useful for the impedance matching that was necessary for high frequency applications. The other useful part of ADS was Momentum. Momentum provides a method-of-moments full wave simulation. This involves performing calculations based off Maxwell's equations for every cell in a mesh that was defined by the user. This provided an overall more accurate simulation than simulations with discrete components like resistors and capacitors.

3.1.2. ViewMaster 8.4

ViewMaster was an ideal layout tool for photolithographic mask development. It allowed for quick and efficient development of masks. Through the use of user defined components, masks could be completely changed by simply changing the components' dimensions. Along with intuitive component placement, editing masks was extremely efficient. ViewMaster output the mask data in gerber format, which was sent to a commercial photoplot manufacturer to procure the mask or mask set. Since the feature sizes of the components were relatively large, a 16,256 dot-per-inch photoplot proved sufficient for fabrication.

3.1.3. Matlab R2010a

Matlab was useful for taking raw data and transforming that data into plots. Matlab provided a high level mathematical tool that could extract data from spreadsheets, perform matrix math with predefined functions, and plot data in many configurable methods. While excel can be used for calculation and plotting, Matlab provided more customization.

3.2. Fabrication Equipment

Several pieces of equipment were used for fabrication. The main pieces of equipment were the HMDS chamber, photoresist spinner, Karl Suss Contact Aligner, and Kepro Bench-top Etcher. Smaller pieces of equipment that were used included a microscope, hot plate, temperature chamber, saw tape applicator, and UV machine.

3.2.1. Hexamethyldisilazane (HMDS) Chamber

The HMDS Chamber provided a reliable method to add a layer of HMDS onto a wafer or substrate. The setup included an air-tight glass container, a wafer holder, and HMDS as shown in Figure 3.1. HMDS was added onto the substrate in order to promote adhesion between photoresist and copper.

Figure 3.1: HMDS Chamber

3.2.2. Photoresist Spinner

The photoresist spinner, as shown in Figure 3.2, provided the ability to evenly spin photoresist onto a wafer or substrate. The spinner had the ability to change

parameters such as revolutions per second, ramp up speed, and duration that would ultimately yield a desired thickness of photoresist evenly over a wafer.

Figure 3.2: Photoresist Spinner

3.2.3. Karl Suss MA/BA6 Contact Aligner

The Karl Suss Contact Aligner, as shown in Figure 3.3, provided the ability to expose photoresist under a mask to ultraviolet light for photolighography. Photoresist that was left unexposed by the mask could then be removed using AZ400K Developer.

Figure 3.3: Karl Suss Contact Aligner

3.2.4. Kepro Bench-top Etcher

After the photolithography process was completed, the unwanted copper was etched by the Kepro Bench-top Etcher as shown in Figure 3.4. The Kepro Bench-top Etcher provided an isotropic copper etch to remove the unwanted copper which etched at a rate of about 1.5 μm per minute. There was a lot of variability in etch rate which was based on a chemical additive and temperature of the chemicals.

Figure 3.4: Kepro Bench-top Etcher

4. Design and Fabrication

In this chapter, design concepts and intricacies associated with software packages are discussed. It begins with setup and simulation of metamaterial transmission lines in ADS. Next, the layout in ADS is presented followed by setting up and running of simulations. Then mask development of the previously simulated layouts is shown in ViewMaster followed by the photolithography process and copper etching.

4.1. Transmission Line

Attached to Agilent ADS, was a program called LineCalc. LineCalc was an essential tool for designing impedance matched lines as shown in Figure 4.1. To design a 50Ω impedance matched line, the following parameters were changed: the relative permittivity, ε_r, of the substrate, height, H, of the substrate, frequency, and the thickness, T, of the metal. Once those values were inputted, the setup was tested by pressing the synthesize button. The line width, W, was updated once the synthesize button was pressed. The line width yielded was the line width needed for the transmission line. For the designs, 4 mil thick LCP with 18 um of copper on each side was used. As shown in Figure 4.1, ε_r = 3.1, H = 4 mil, T = 18 um, Freq = 8 GHz, and Z0 = 50Ω were the input parameters which yielded that the width of the copper trace needed to be approximately 232 μm. These parameters were used for the rest of the simulations in ADS.

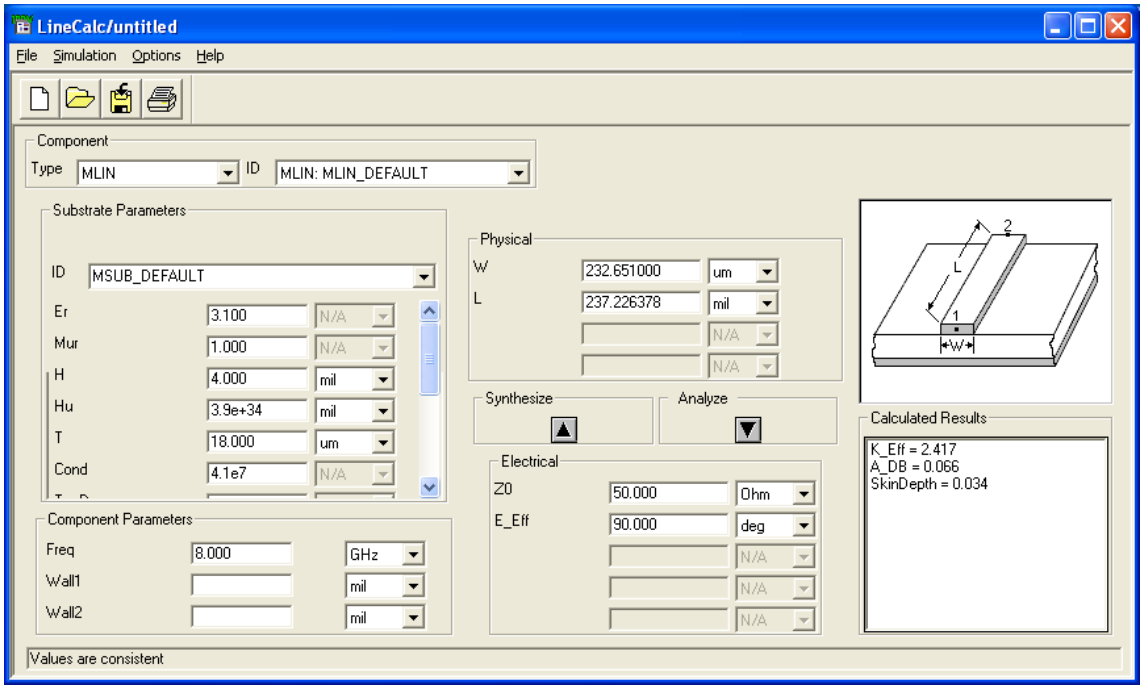

Figure 4.1: ADS Linecalc Software

4.2. Metamaterial RF Simulation

ADS software was useful for high frequency testing of metamaterial structures. Via the layout tool provided in ADS, metamaterial structures could be built for simulation relatively easily but with some unusual tactics for placement. The layout tool provided basic structures that could be dragged and dropped into the layout. The basic structures that were of use were drawing lines of fixed widths, chopping blocks, drawing basic geometric shapes, and building curves of fixed widths.

While the necessary components for constructing SRRs and CSRRs were available in layout, the components had to be manipulated and were anything but convenient for placement. This was especially true when compared to ViewMaster.

When drawing lines of fixed widths, they had to be carefully drawn and were not snapped automatically onto an axis or grid. If a desired length of line was needed, that number could not be manually entered even though it was clearly displayed in the properties of the line. Instead, the line had to be manually extended while keeping on the axis that shouldn't vary. As an example, while the line was extended in the x direction, the y direction would shift by several pixels. Aside from simple line placement, there was no point of reference to line all of the components up with for placement. In order to line components up accurately, the resolution had to be small in order to adjust components a few microns at a time. However, when zoomed in close enough to see the tic marks, an overall view of the components was lost. This would result in offsets in the off-axis direction. Once a CSRR structure was built, block chopping had to be utilized in order to create a reproducible block. Once a reproducible CSRR block, shown in Figure 4.2, was built, a CSRR transmission line was easily constructed as shown in Figure 4.3.

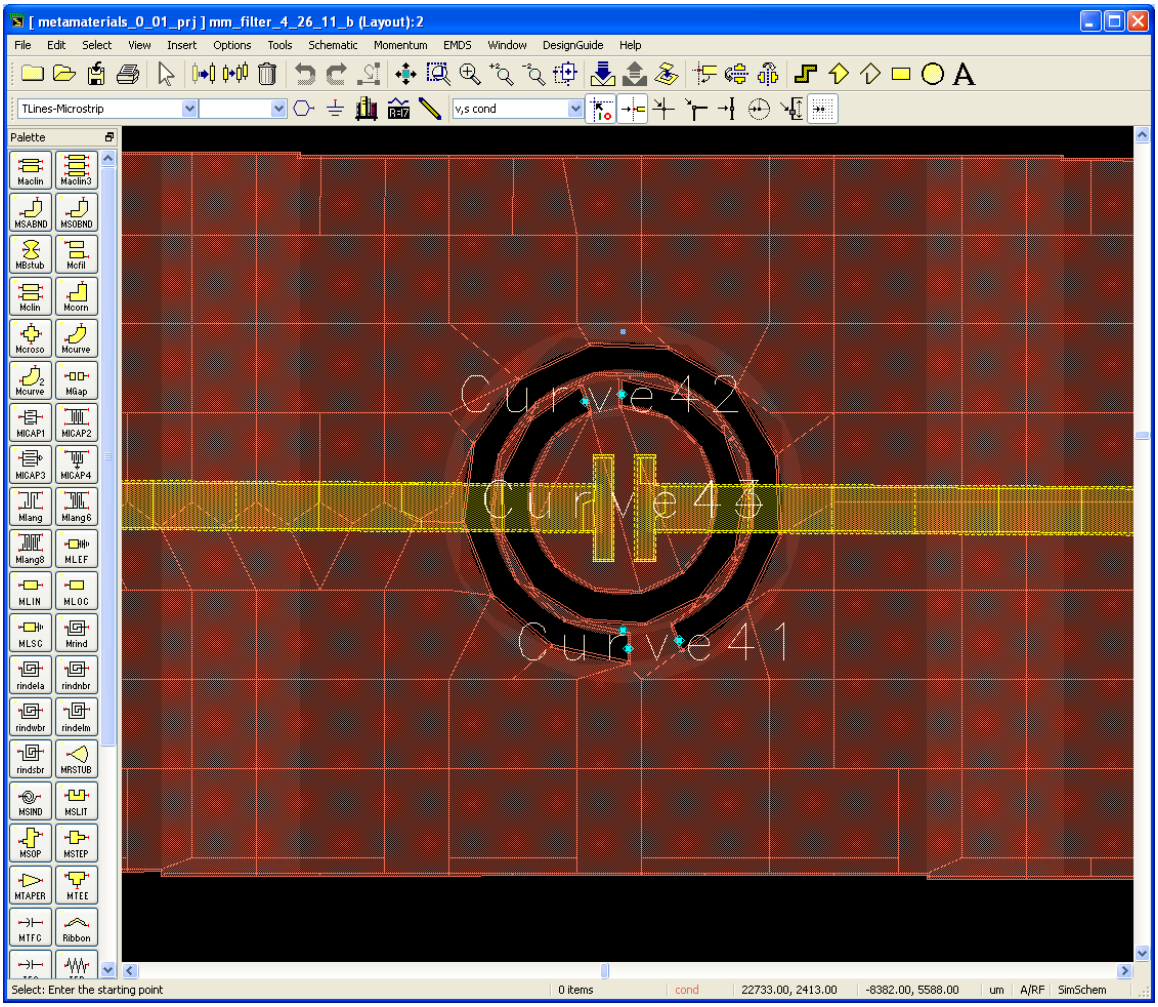

Figure 4.2: ADS Single CSRR Design

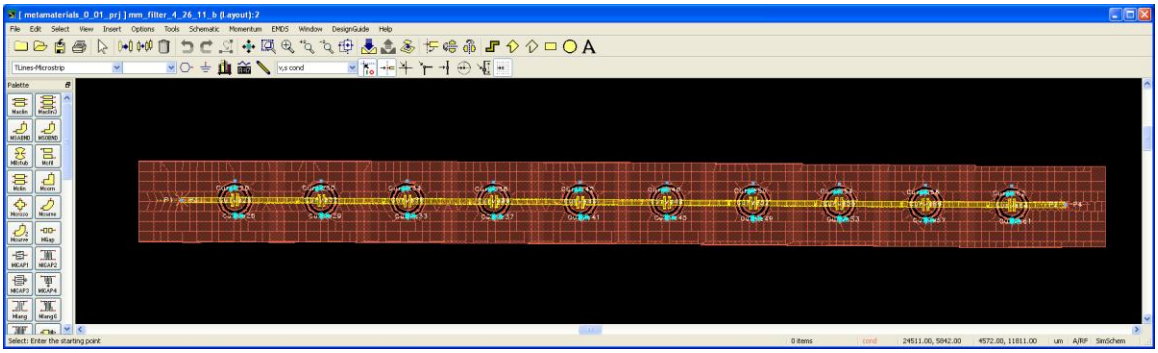

Figure 4.3: ADS Multi-cell CSRR Design

Once the structure was completely designed, 50Ω ports were added to the signal lines on each side of the metamaterial filter. For a finite ground plane, ground reference ports needed to be added onto the ground plane [18]. In order to add a ground reference port, add a port onto the ground layer and go to ADS → Momentum → Ports → Editor. From the port editor, the port can be changed to a "Ground Reference" port instead of the standard internal port and attached to another port by entering its number. An example of the ground reference port placement is shown in Figure 4.4. Next, the simulation parameters needed to be updated. Under ADS → Momentum → Create/Modify Substrate, the thickness of the metal and substrate could be updated as well as the organization of the substrate layers. An example can be seen in Figure 4.5 and Figure 4.6 of the substrate layers and layout layers respectively. Once the substrate was setup, the mesh density was edited through ADS → Momentum → Mesh → Setup. The mesh was designed for the top frequency and the Cells/Division was set to a reasonably high number of 30 to 50 as shown in Figure 4.7. In order to deal with the rings from the CSRR, the arc length needed to be lowered to give more cells around the rings. This was accomplished by lowering the arc resolution. Figure 4.8 shows a mesh of 30 cells per wavelength. The higher the density, the longer the simulation took; however, the results became more accurate. After the mesh setup, the S-parameters were updated as shown in Figure 4.9. The desired frequency range, file name, and number of points per decade were changed in this menu. A few things to note are that the results of the simulation will be associated with the file name but not the original layout. Good notes were taken to associate layout and simulation results. The tab for ADS → Momentum needed to read

Momentum and not Momentum RF. This was because regular Momentum was built for sub-wavelength circuits and did not make certain necessary assumptions. Once everything was setup and run, the results could be displayed, as shown in Figure 4.10.

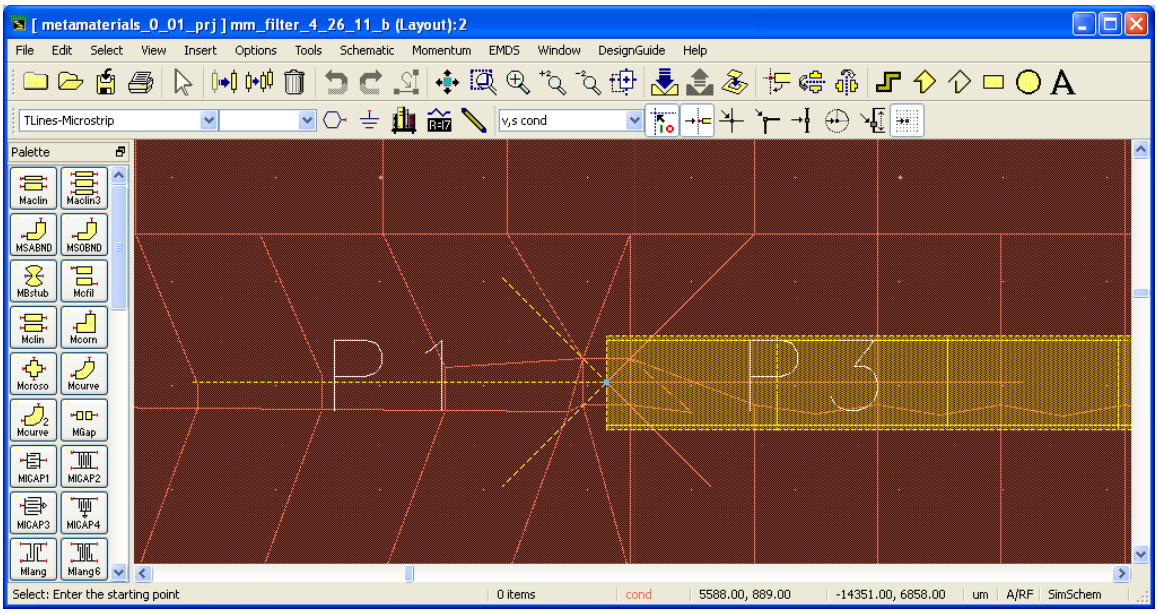

Figure 4.4: ADS Ground Reference Ports

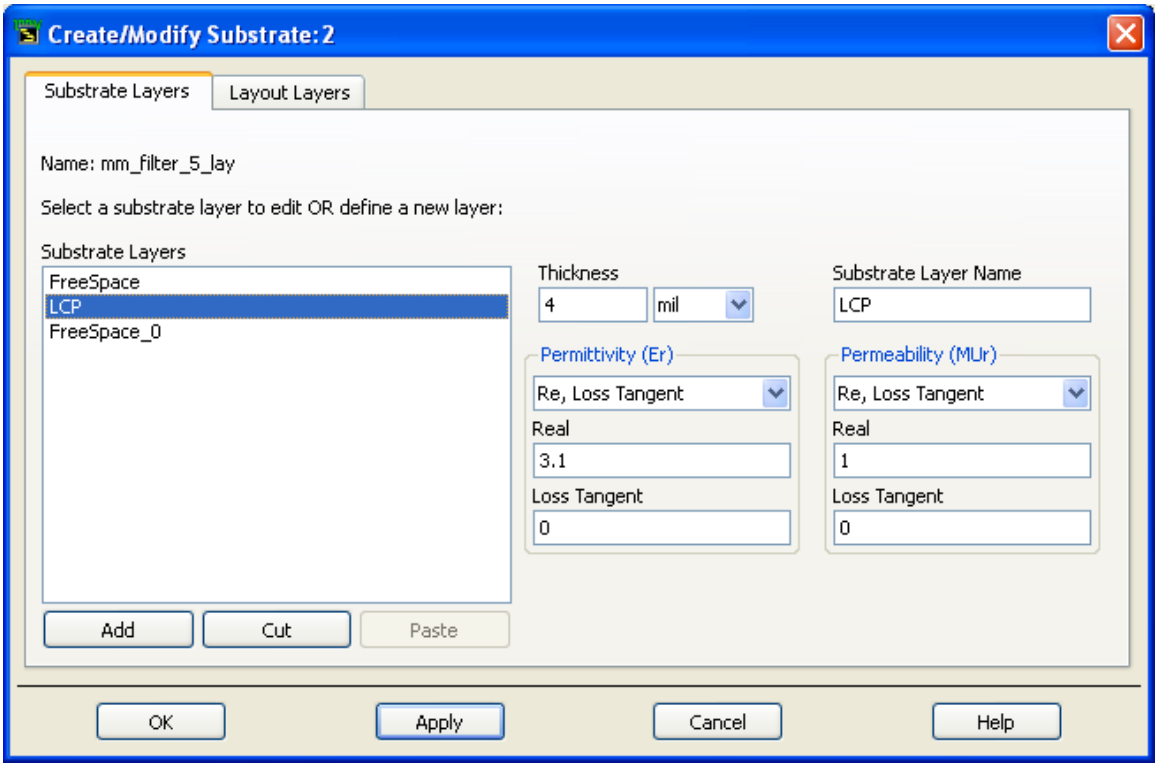

Figure 4.5: ADS Simulation Substrate Layers

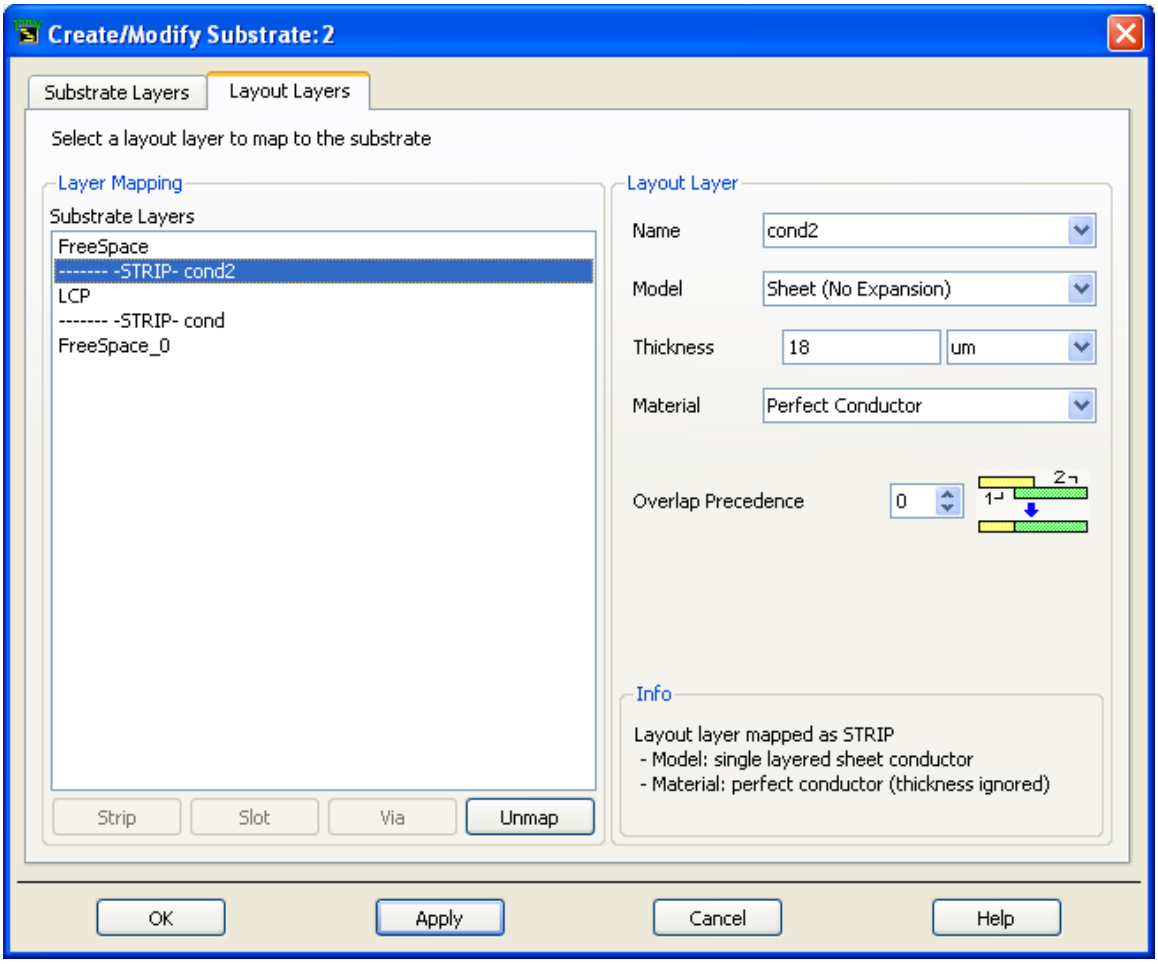

Figure 4.5

Figure 4.6: ADS Simulation Layout Layers

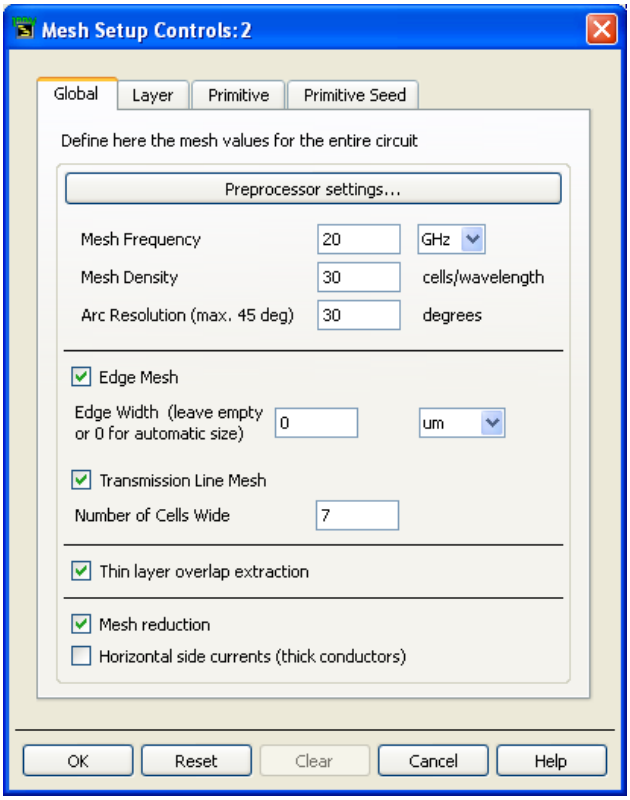

Figure 4.7: ADS Simulation Mesh Setup

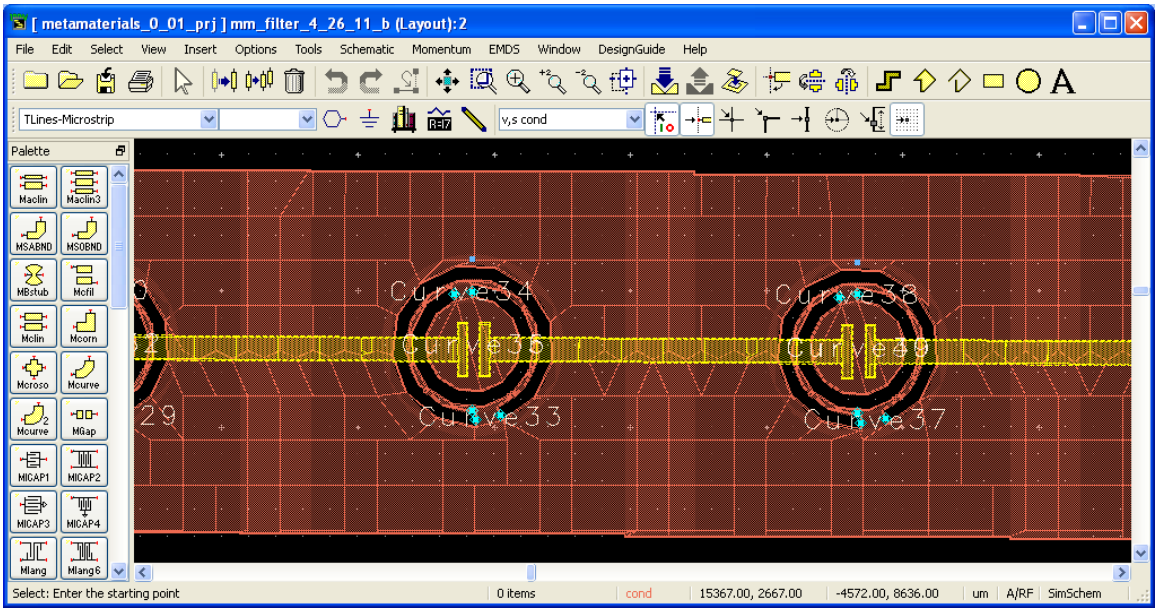

Figure 4.8: ADS Mesh Preview

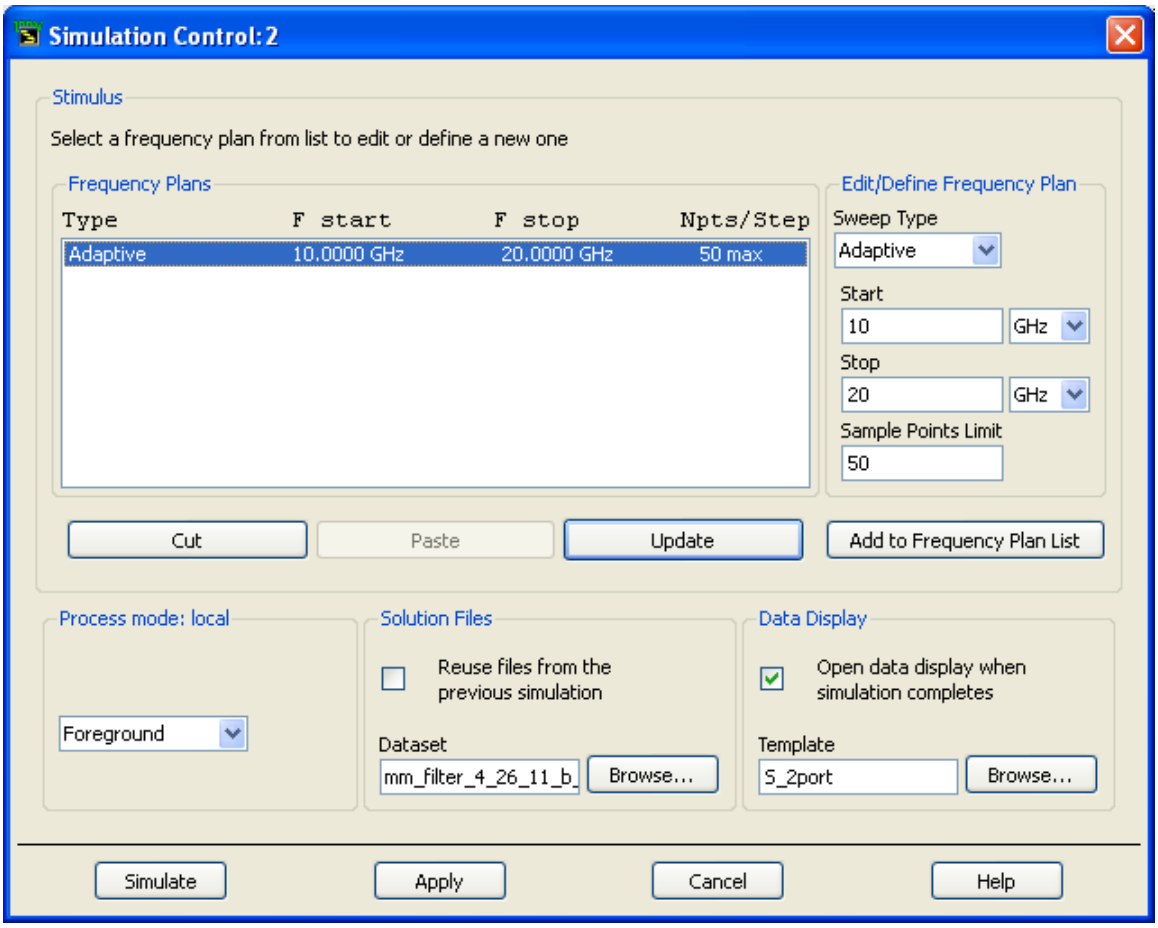

Figure 4.9: ADS Simulation S-Parameters

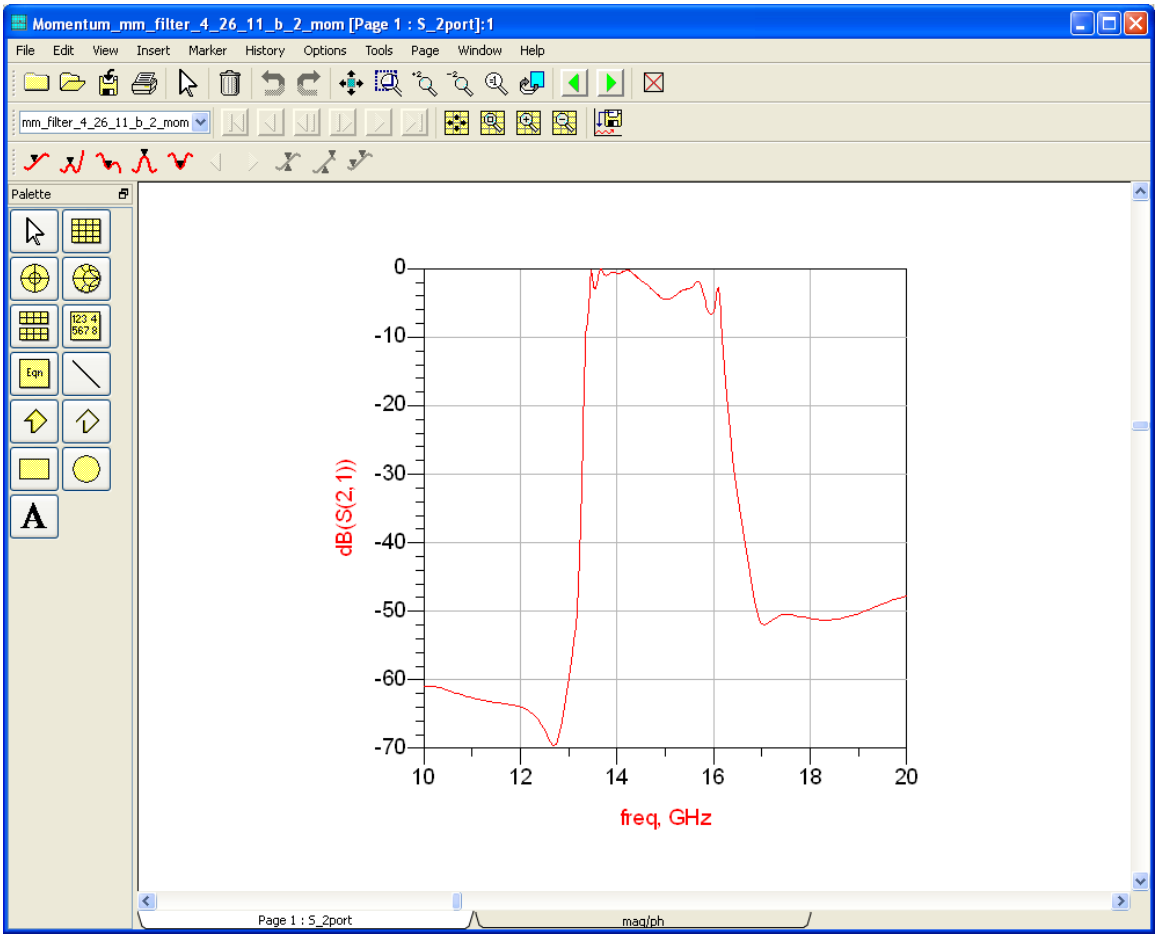

Figure 4.10: ADS Simulation Results

To provide a visualization of the layout, ADS had a 3-D visualization tool. This tool was convenient for double checking layout design, but served no simulation purpose. To access the 3-D visualization tool, ADS → EMDS → 3D EM Preview was selected. Once selected, a 3-D scale view of the layout was generated. An example of a generated 3-D preview is shown in Figure 4.11 and 4.12.

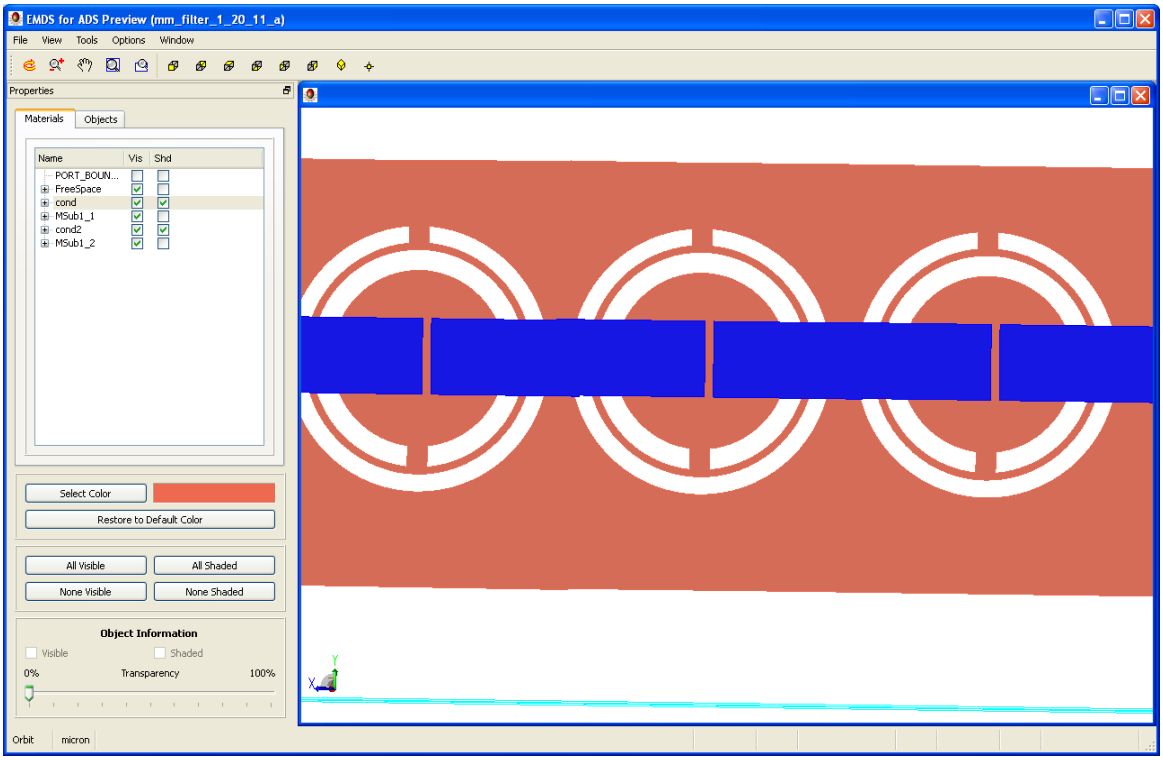

Figure 4.11: ADS 3-D Preview (Top)

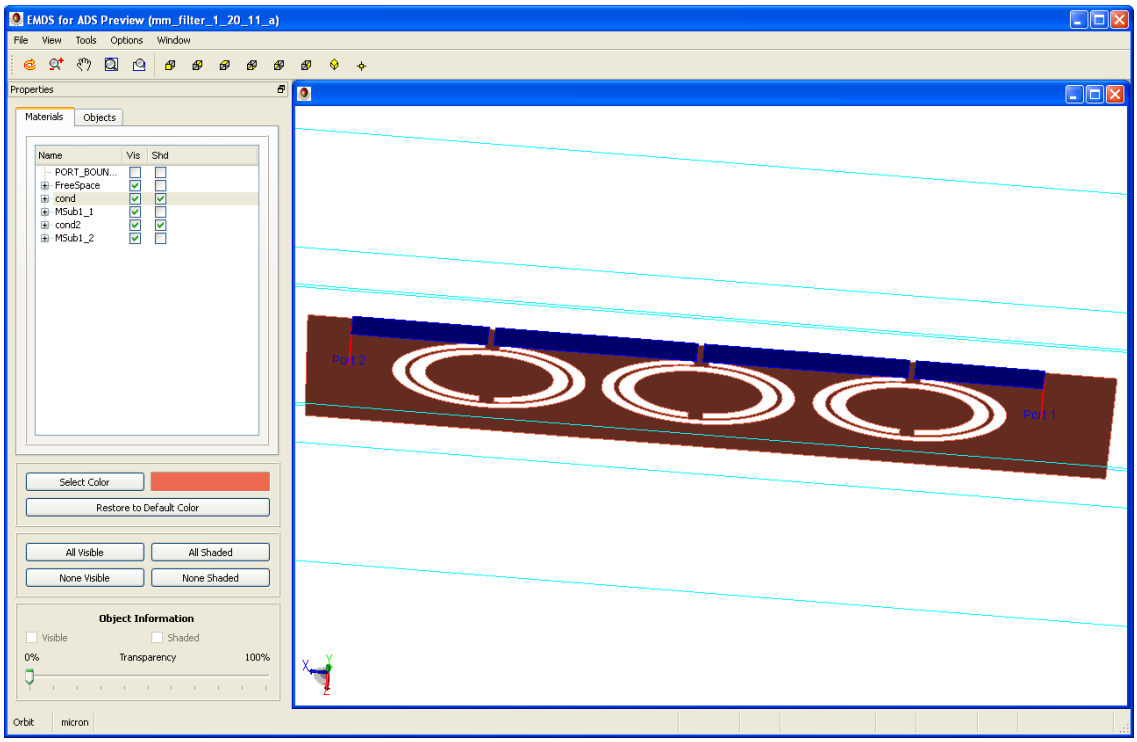

Figure 4.12: ADS 3-D Preview (Side)

4.3. Mask Development

Once the simulations were completed, masks could be designed in ViewMaster. Each mask was created on a separate layer. On the first layer, a four inch circle was placed in order to visualize the size used for fabrication, as shown in Figure 4.13 by the giant green circle. This put the size of components in comparison to a 100mm diameter Si wafer and helped avoid overly large masks. Next, construction of a single CSRR cell was made. An example of a CSRR cell is shown in Figure 4.14. Since the wet copper etchant was isotropic, a buffer of 25 μm was added to each edge of the mask that would be exposed when etching. This was needed since copper etching would undercut the mask by more than the thickness of the copper, which was 18 μm. With undercutting

being considered, the CSRR rings were easy to construct with base components of solid circles and circles with a circular hole removed. Once one CSRR structure was built, the gaps between the rings were measured to verify that the distances were correct before etching.

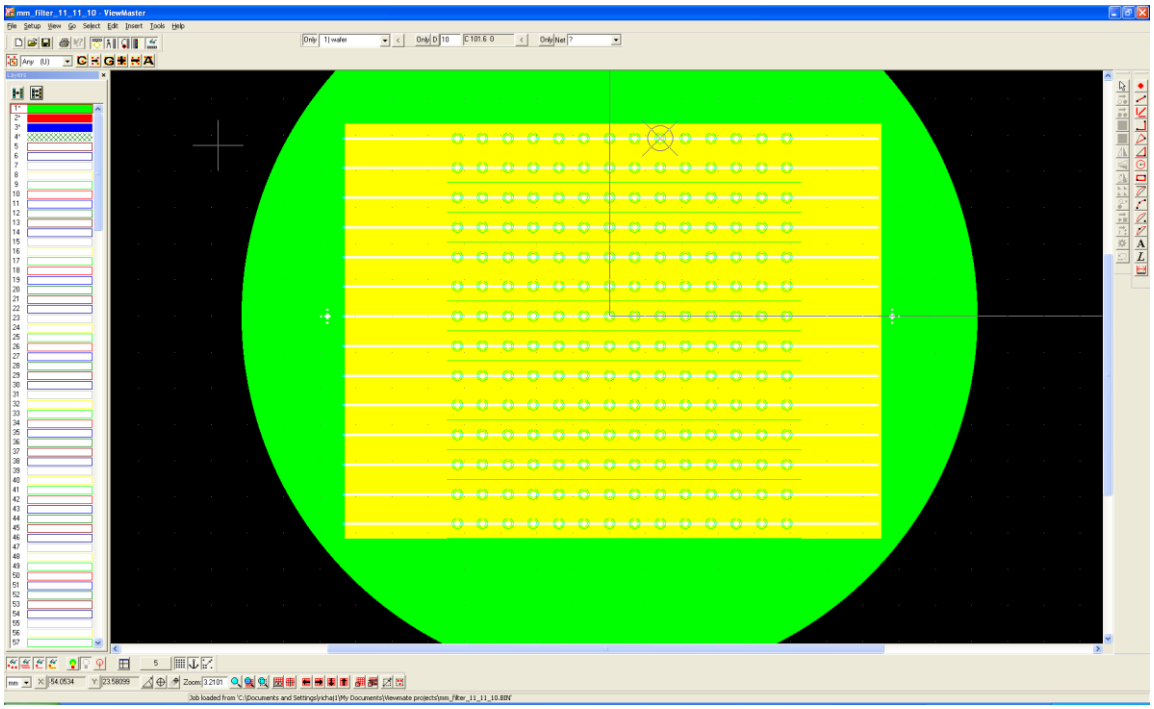

Figure 4.13: ViewMaster Wafer Layout Overview

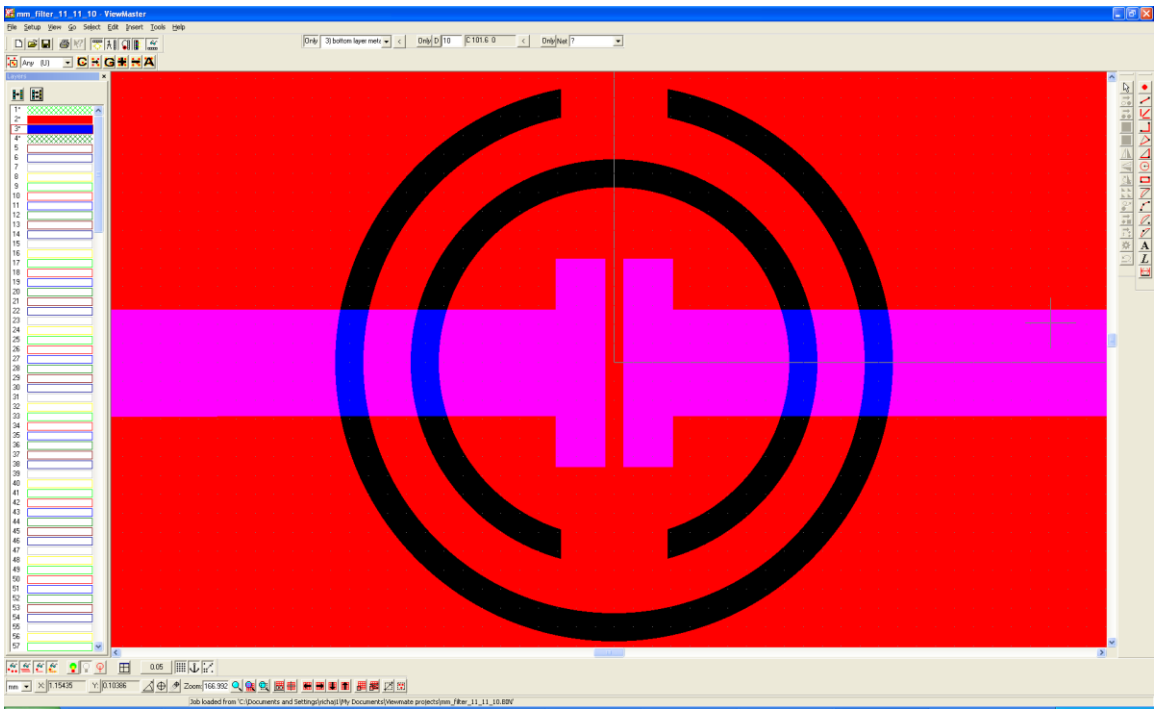

Figure 4.14: ViewMaster CSRR Cell

After developing the single CSRR cells that were desired, an overall design was put together. For several cases, this involved connecting the same cell together with nearly as many as could fit onto a wafer, as shown in Figure 4.15. Next, extra long lines were added at the end of each metamaterial transmission line in order to make it easier to solder sma connectors for testing purposes. Finally, alignment marks were placed to ensure both layers were properly aligned. An example of alignment marks is shown in Figure 4.16.

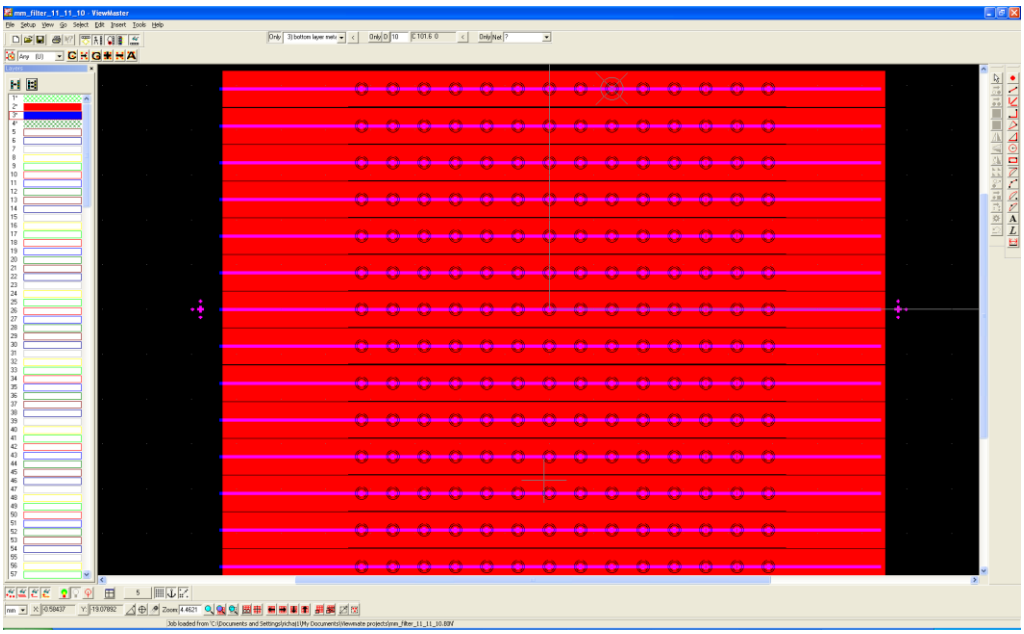

Figure 4.15: ViewMaster CSRR Cell Arrays

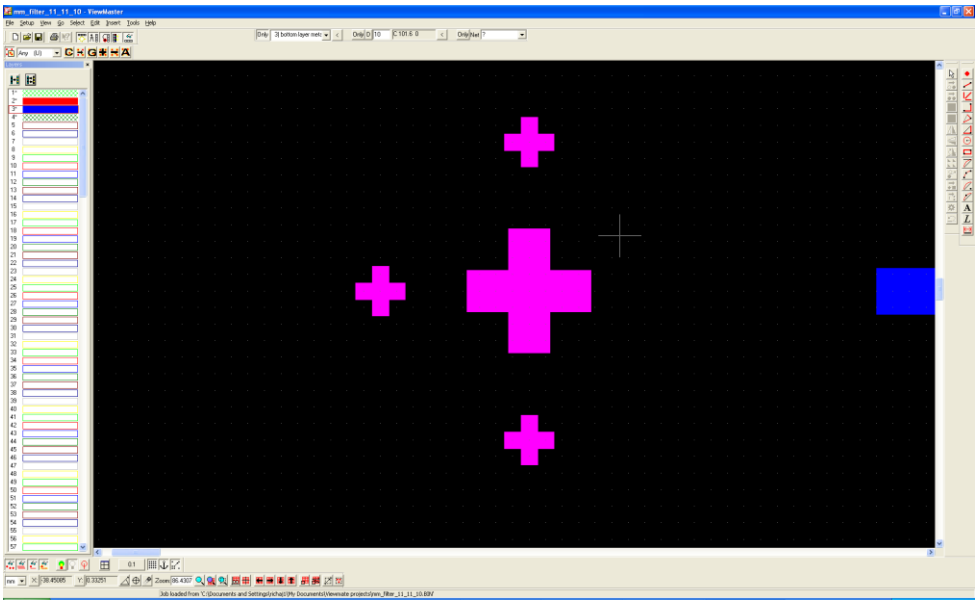

Figure 4.16: ViewMaster CSRR Alignment Marks

4.4. Photolithography and Copper Etching

Once the photoplot masks were developed, ordered and received, fabrication could be performed. An overview of the complete process can be found in Appendix A. First, the wafer sized LCP substrate needed to be cut from a sheet of LCP. This was accomplished by tracing an exacto knife around a dummy 100mm diameter silicon wafer which ensured a near perfect 4 inch diameter circular substrate. Once cut, the LCP substrate was transported to the lab.

Once in the lab, the LCP substrate was cleaned in a 5% HCl bath for 60 seconds. After the bath, the LCP substrate was rinsed in deionized water and immediately dried with compressed air. Next, the LCP substrate was dehydrated in a temperature chamber at 120° C for 20 minutes. Note that the LCP substrate needed to cool for up to 5 minutes in order for the next step to work properly. After cooling, the LCP substrate was placed in the HMDS chamber for 10 minutes. Adding fresh HMDS helped discourage photoresist from being removed during development. After applying HMDS, photoresist was spun onto the LCP substrate. Since the LCP was flexible, there was a tendency to lose vacuum on the photoresist spinner. If loss of vacuum occurred, the LCP substrate was flexed and retried. This was repeated until a reliable vacuum was made before photoresist was added. After photoresist was properly added, the LCP substrate needed to be softbaked at 105° C between 60 and 90 seconds. It was important during softbaking to keep as much LCP as possible in contact with the hot plate. Multiple tweezers were used to hold opposite sides down to the hot plate. Once completed, the LCP substrate could be exposed to ultraviolet light via the mask aligner. For the mask aligner, loss of

vacuum was irrelevant. However, it was important to manually move the LCP substrate to locate the mask in the middle of the LCP substrate before exposing. In order to maintain structural integrity, the mask that yielded the most copper after etching was used first. After the photoresist has been exposed in the contact aligner, the photoresist was developed. This involved placing the exposed LCP substrate in a two to one mix of water to AZ400 Developer for two minutes. While in the mixture, the liquid was constantly agitated to promote uniform development. Next, the LCP substrate was rinsed with deionized water and dried with compressed air. Once dry, the mask was carefully inspected under microscope to ensure the mask was fully developed and that no serious defects occurred during the previous photolithography process. Once visibly checked, saw tape was attached to the non-developed side of the substrate to protect the copper on that side during etching. Finally, the copper could be etched off the wafer with the Kepro Bench-top Etcher. Etching the copper as soon as possible after performing the photolithography process would help avoid imperfections caused by debris settling onto the mask. In order to provide a more uniform etch across the LCP substrate, it was rotated several times in the Kepro Bench-top Etcher. Figures 4.17 and 4.18 show both sides of a CSRR after the etching process.

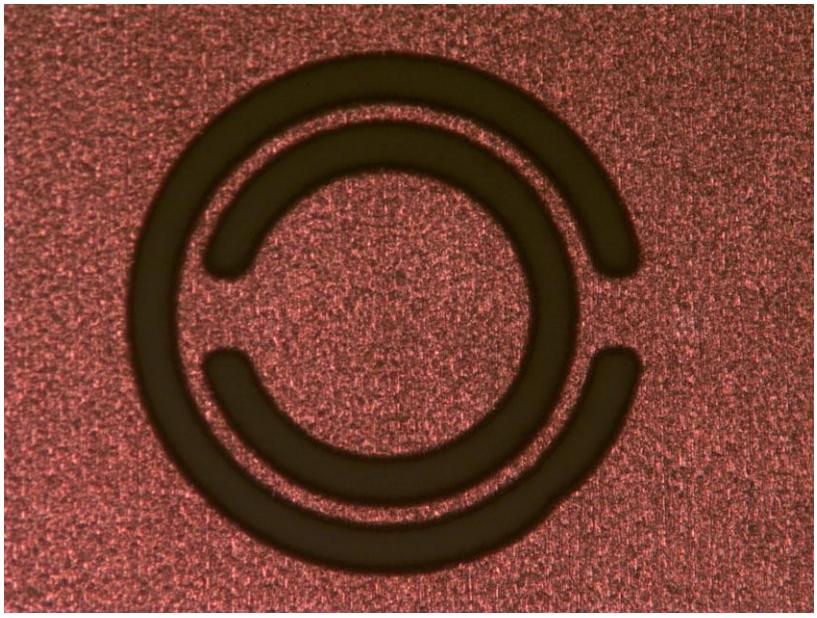

Figure 4.17: LCP CSRR Ground Layer

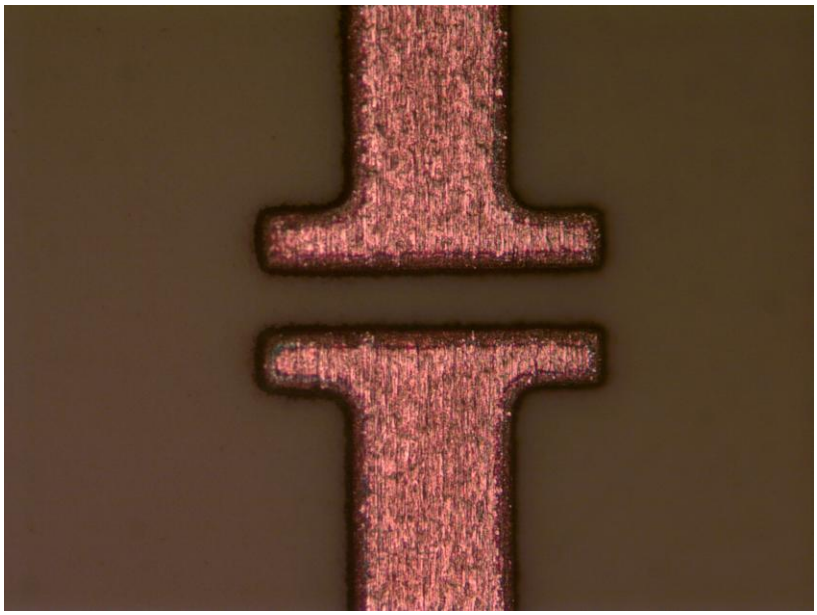

Figure 4.18: LCP CSRR Transmission Line Layer

Once the LCP substrate was etched on one side, the saw tape was exposed to ultraviolet light for 20 seconds to break adhesion. Then the saw tape was removed.

Next, the substrate was run through steps 2 thru 9 which encompasses the photolithography process. Additionally, if there was an issue at the end of the photolithography process and saw tape was already placed without etching copper, the saw tape needed to be removed before re-doing the photolithography process. After both sides of the LCP substrate were etched, the photoresist was removed. This involved rinsing acetone over the LCP substrate followed by alcohol and DI water. Finally, the substrate was dried with compressed air.

One of the big issues with wet copper etching was that it was isotropic. At smaller depths of copper of a few thousand angstroms, this was not an issue. However, when the depth of copper was 18 μm, a large variance potential and overetching was introduced. To counteract these issues, a 25 μm buffer was introduced and substrate rotation was utilized during copper etching. Unfortunately, there were still variances of several microns and even tens of microns across the substrate and undercutting could be upwards of 40 μm before the entire substrate was etched entirely.

4.5. Alternate Copper Etching

An alternate method for etching copper was utilized. It provided more accurate etching at the cost of longer durations of etching and more expensive chemicals. First, a bowl was placed onto a hot plate with a spinning mechanism. This bowl was filled with copper etchant and brought to 40° C. Once the temperature stabilized, a small magnetic rod was carefully lowered into the bowl. Then the spinning mechanism was turned on to provide a low rpm spin with the magnetic rod. Next, the LCP was placed on top of the copper etchant with the exposed side face down. Due to the thick surface tension of the

copper etchant, the LCP would float on top while being spun. The LCP would stop floating if there were too much speed produced by the spinning mechanism. When the LCP stopped floating, it would bang erratically against the sides of the bowl. By keeping the rpm low enough, the LCP would float softly on top of the copper etchant while being uniformly etched.

4.6. LCP Etching

After the copper was etched, the LCP etching process could begin. Note that LCP would only etch where copper had already been removed. First, the LCP substrate had leftover photoresist removed and was dehydrated at 120° C for 20 minutes. Then an aluminum layer of 5000 Å was added onto the wafer. The aluminum layer was added using E-beam deposition. Once the LCP had an aluminum layer, a photoresist mask was placed onto the aluminum using the photolithography process described earlier. Once patterned, the aluminum was etched in AZ400K Developer because of its selectivity against copper and for aluminum. Next, the LCP was etched with an oxygen RIE process [5]. The etch rate was slightly less than one micron per minute. Lastly, the aluminum mask was completely removed with AZ400K Developer.

5. Metamaterial Filter Testing

When fabrication of the LCP wafer was complete, the metamaterial filters were thoroughly tested. The test setup involved cutting the LCP substrate into transmission lines and soldering sma connectors onto the lines. Once setup was complete, actual testing involved measuring the devices with a network analyzer. Finally, the results were saved from the network analyzer and displayed via Matlab.

5.1. Test Preparation

After fabrication was complete, the LCP substrate needed to be cut. Since the device sizes were relatively large and LCP was flexible, they could be manually cut with scissors. If a non flexible substrate were used, a machine would be needed to dice it, requiring a backing wafer as well. Since the LCP substrate could be manually cut, dicing lanes were designed into the mask in order to aide the cutting process. Once one strip of transmission line was cut, sma connectors were carefully soldered onto it. Because the transmission line width was 230 μm, the traces had a tendency to pull off easily during testing and soldering. To avoid pulling traces off during soldering, the ground plane was soldered first followed by the transmission line. The solder contacts were verified with a microscope. Due to these issues, an alternative to soldering sma connectors onto the substrate was pursued. The alternative involved end launch sma connectors that clamped

down onto the device. End launch connectors were chosen because they helped avoid pulling off the traces and difficulty soldering.

5.2. Network Analyzer Testing

Next, the metamaterial transmission line was tested with an HP8510C network analyzer, HP8517B S-Parameter Test Set, and HP83651A Synthesized Sweeper. The network analyzer was first calibrated using an open circuit, a short circuit, and a 50Ω termination. The S11 of the thru measurement after calibration was less than 40 dB. The ripple in the S22 of the thru measurement after calibration was less than 0.05 dB.

After calibration was complete, the metamaterial filter was connected. Since the LCP was flexible and the sma cables were rigid, there was a lot of bending and torqueing of the system. The first test involved keeping the sma cables pulled apart with enough force to keep the metamaterial filter taught and straight. Then the s-parameters were captured. It was important to not physically touch the sma connectors or filter during data capture in order to avoid affecting the system with stray capacitance.

Next, the flexibility of LCP was evaluated. Tests were run with respect to the transmission line's orientation and various radii of pvc pipe. All of the tests were run using the outside of the pvc pipes and thus are convex. A full set of tests were run for the transmission line pointing up from the pvc and down from the pvc. Initially, the filter was laid flatly on a piece of pvc pipe, as shown in Figure 5.1. The flat test provided a calibration for the flexed tests because the dielectric change between air and pvc would affect the filter's resonance frequency. Pvc has a dielectric that changes drastically with frequency but can be estimated to be around 3 [35]. Once the flat data was captured, the

LCP was flexed over various sized pvc pipes, as labeled in table 5.1, with both sides of the LCP in contact with the pvc. The data from the flexing over pvc pipe was then compared to the flat pvc test as shown in Figures 5.2 and 5.3.

Table 5.1: Test number to PVC diameter correlation

Number	1	2	3	4	5	6
PVC Diameter	1/2"	3/4"	1"	1 1/4"	1 1/2"	2"
Radius of Curvature in inches	0.542	0.65	0.804	0.984	1.115	1.3585

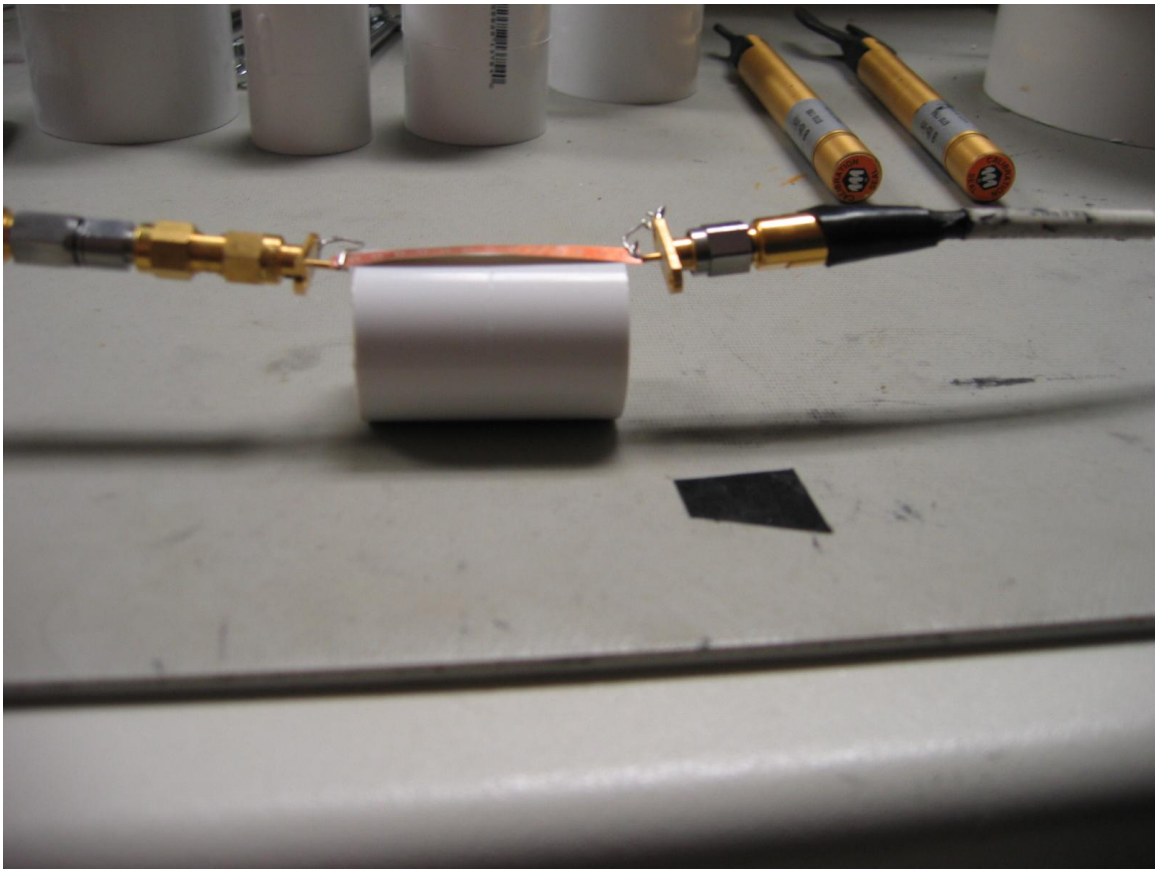

Figure 5.1: PVC Calibration

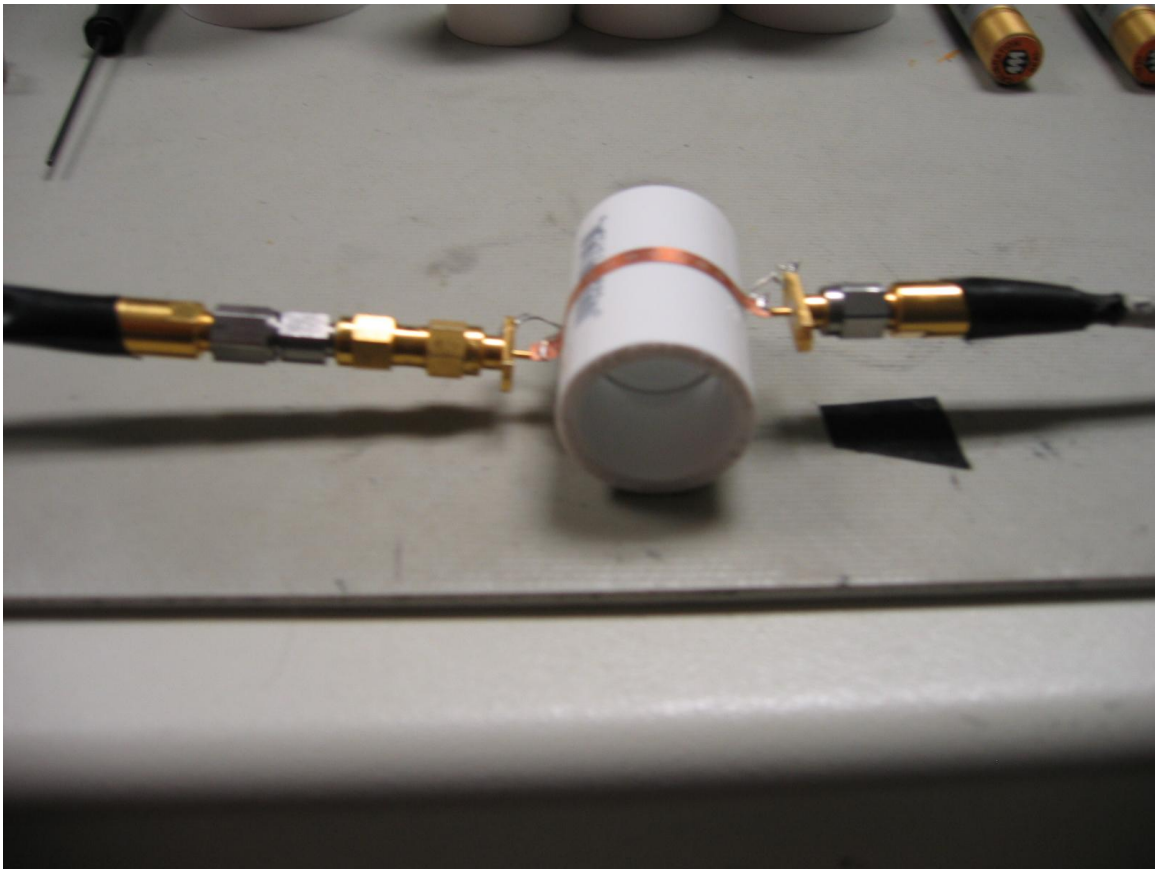

Figure 5.2: ¾” PVC Flexibility test

Figure 5.3: 2” PVC Flexibility test

5.3. RF Filter Results

After the tests were run and data captured, the plots of the data were compiled in Matlab. Figure 5.4 shows the ADS simulation data compared to two separate filters in open air. The frequency mismatch is associated with the etched filters having different dimensions than the simulation. Figure 5.5 shows two separate filters laid flatly on a pvc pipe with both transmission line orientations. As shown in Figures 5.6 and 5.7, the flexing of the filters transmission coefficient, or S21, had little to no affect on the resonance frequency of the structures. Figure 5.6 shows the tests for the transmission line pointing up while Figure 5.7 shows the tests for the transmission line pointing down. The

transmission coefficient yielded a very prominent passband filter between 14 GHz and 16.25 GHz. There was significant ripple in the passband region which can be attributed to pvc behaving non-uniformly at the frequencies of interest. The passband ripple was not as prominent but was still severe when the filter was surrounded by air. Figure 5.8 and 5.9 clearly show a strong reflection coefficient at 16 GHz regardless of transmission line orientation or flexing of the substrate.

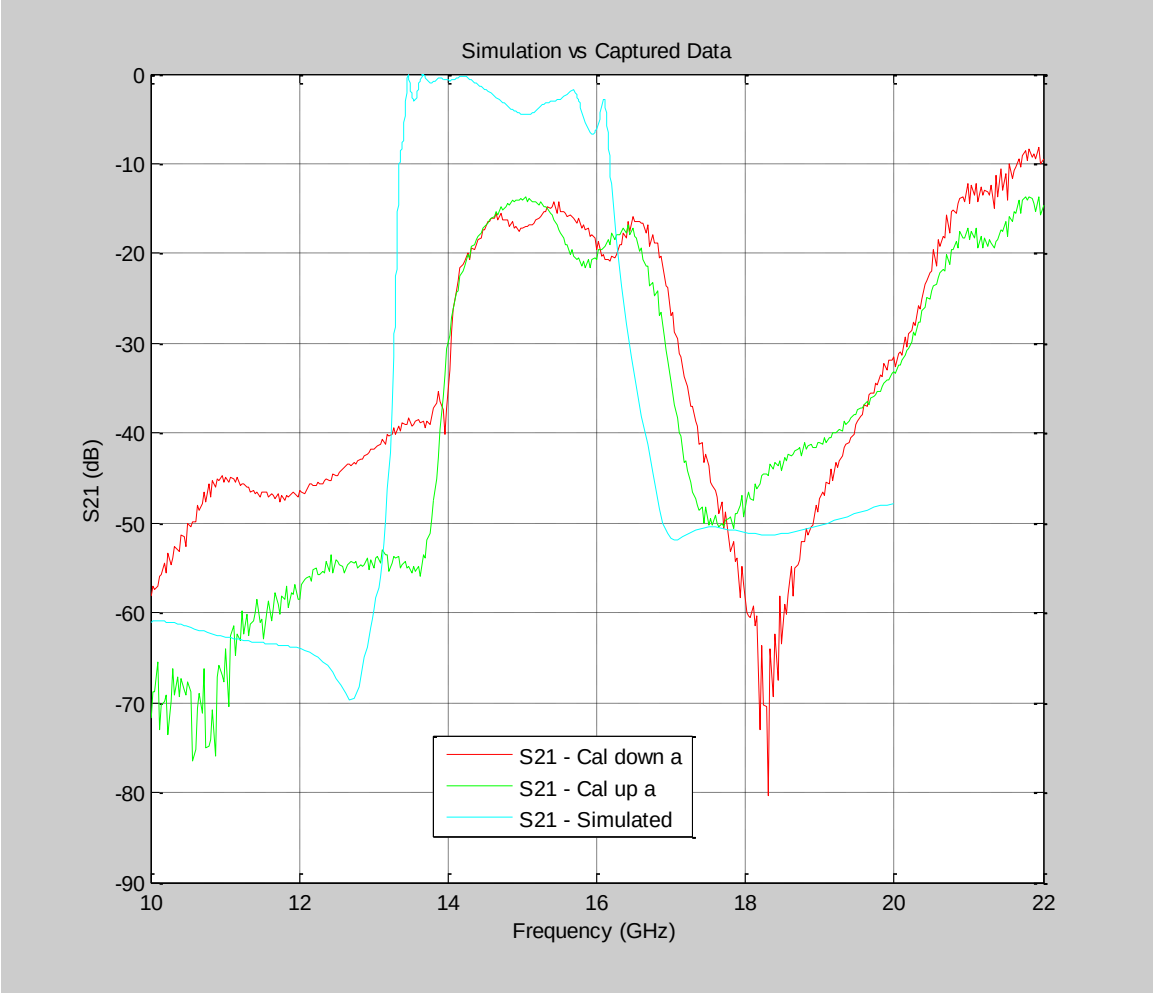

Figure 5.4:S21 of Simulated vs Captured Data

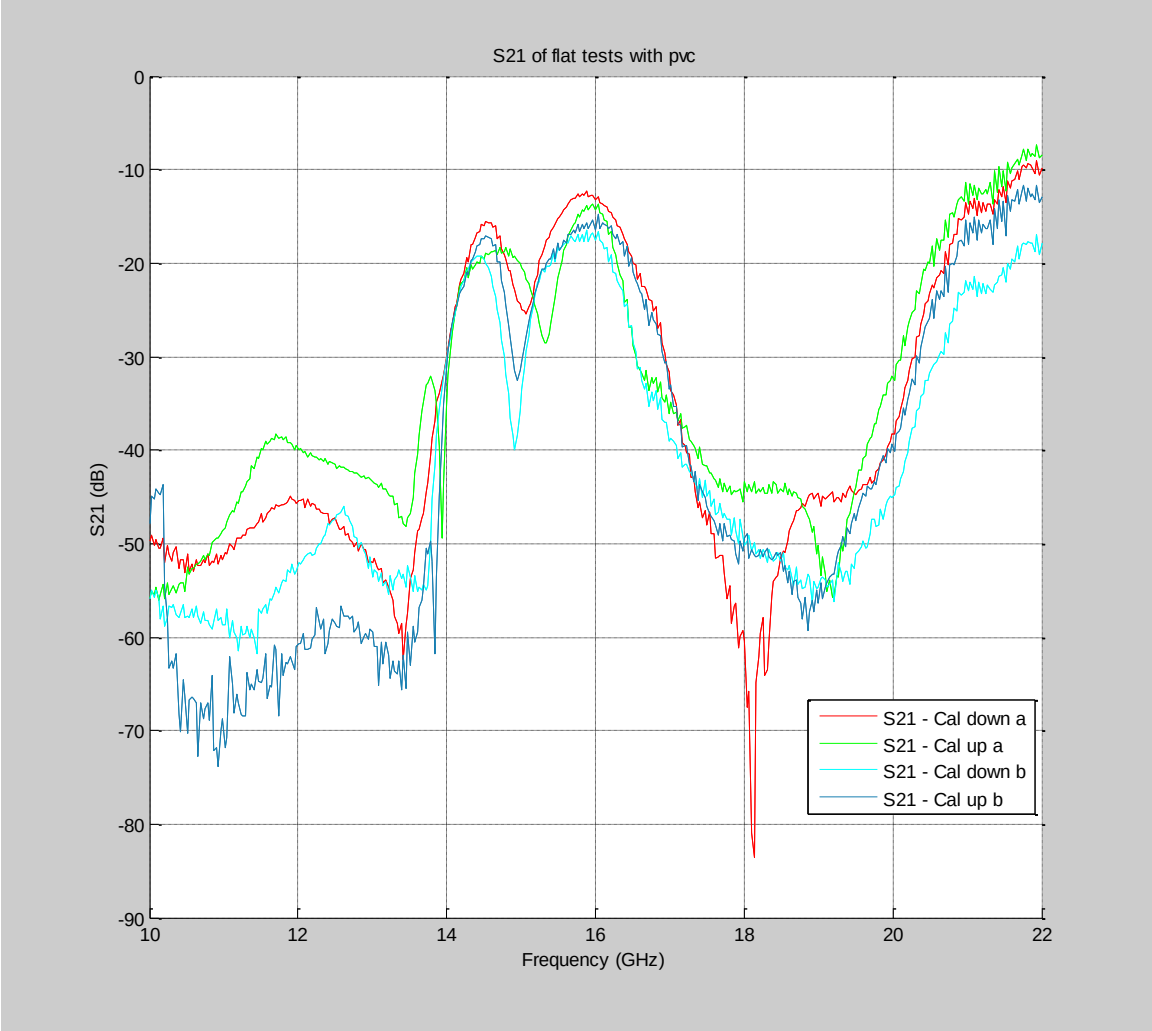

Figure 5.5:S21 of flat tests with pvc

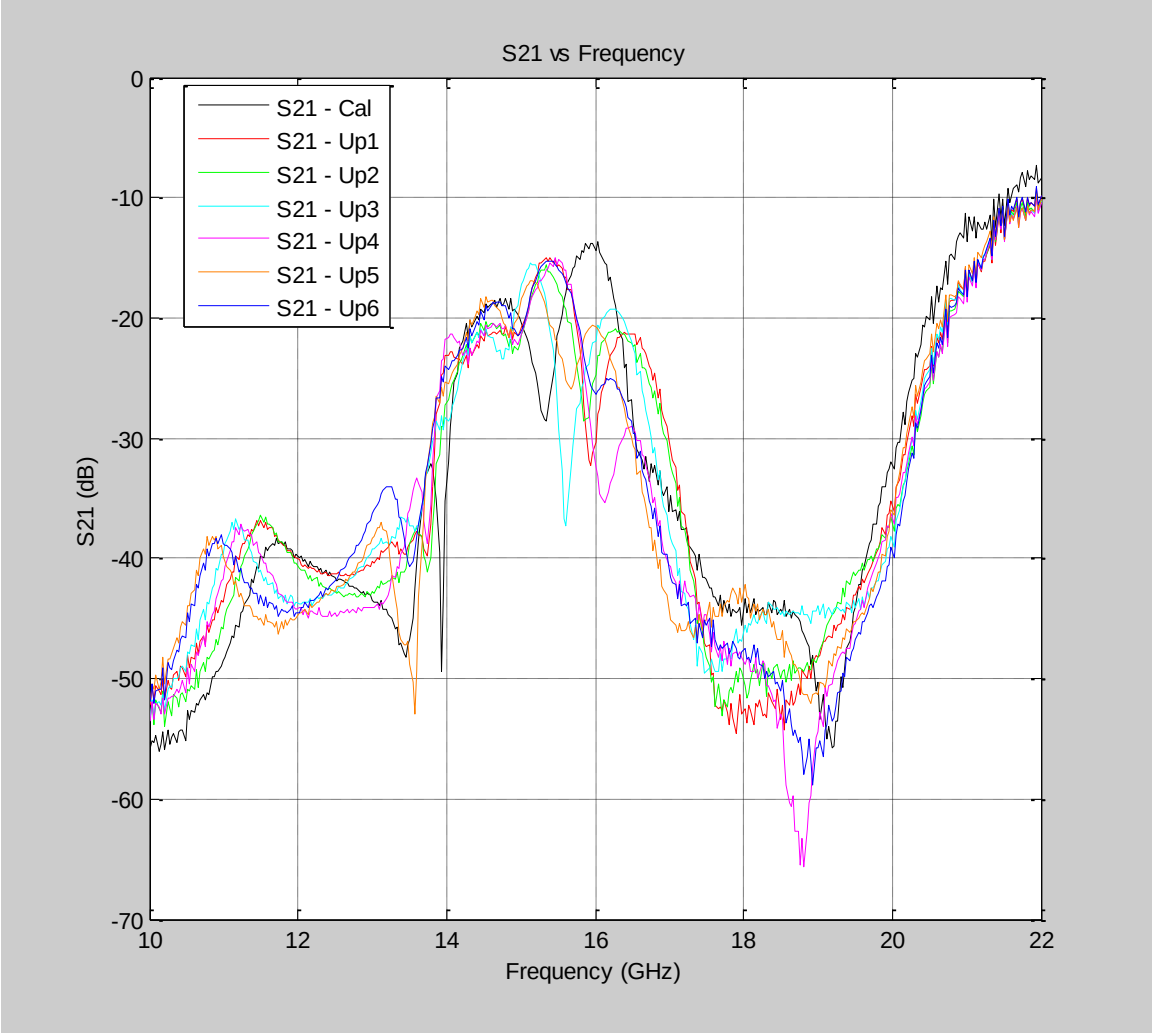

Figure 5.6: S21 PVC Flexibility T-line up

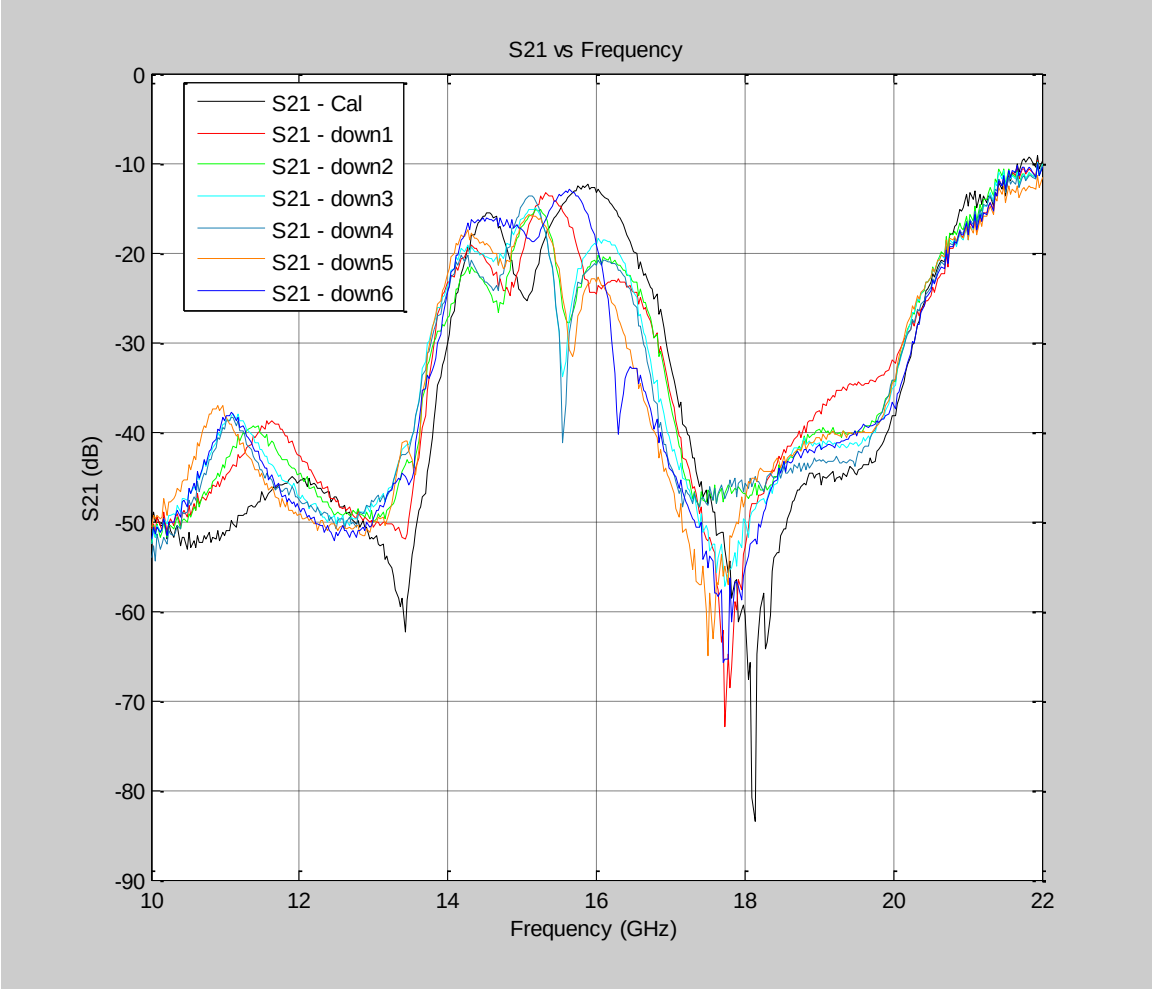

Figure 5.7: S21 PVC Flexibility T-line down

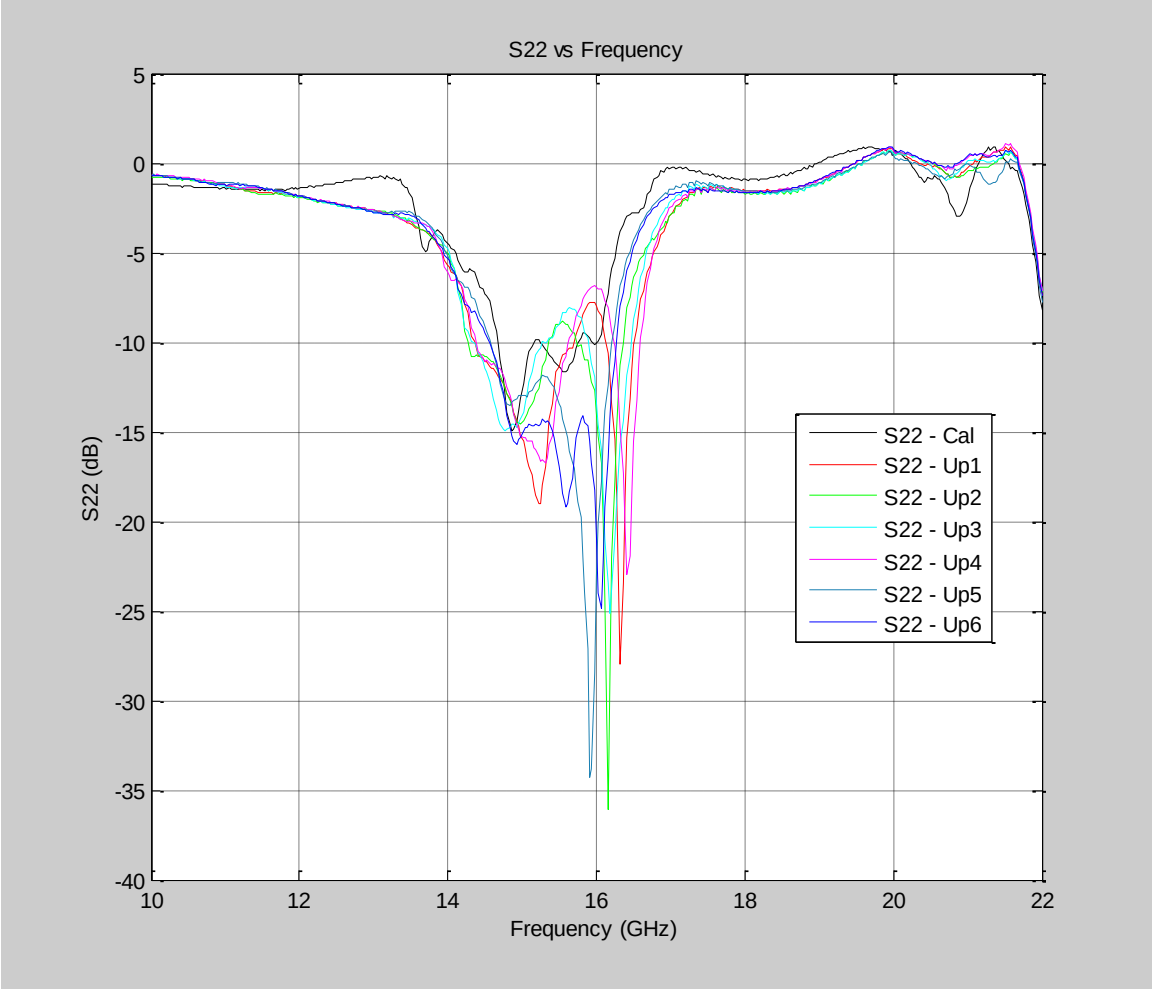

Figure 5.8: S22 PVC Flexibility T-line up

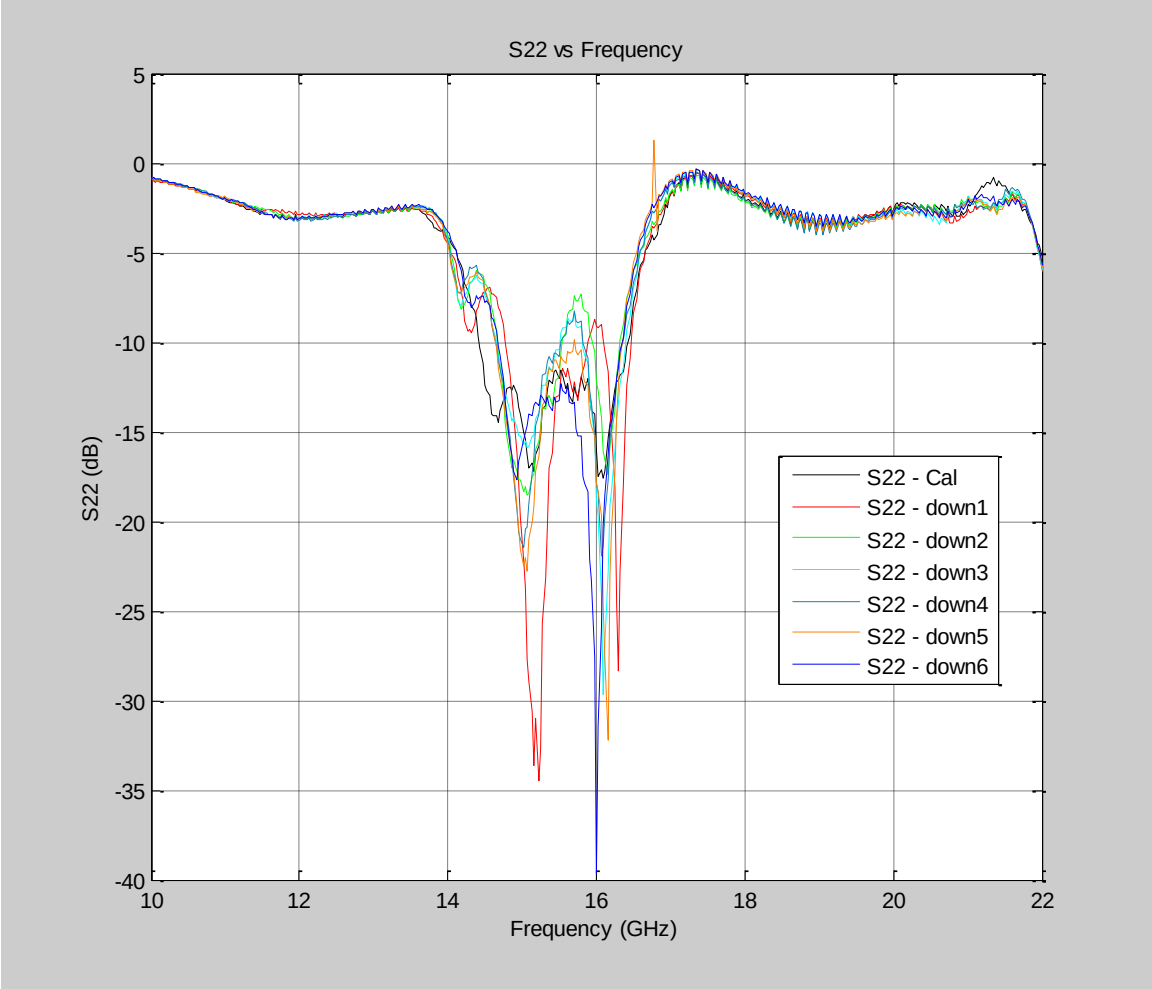

Figure 5.9: S22 PVC Flexibility T-line down

As previously stated, there was a significant amount of non-uniformity of copper etching on a single substrate. In Figure 5.10, the S21 of two sets of 13 cell CSRR filters are shown. They were cut from the same LCP substrate. The filters had a difference of several microns of copper which resulted in slightly different resonant frequencies.

The passband of the filters had a significant amount of attenuation. As shown in Figure 5.10, having less CSRR rings provided less attenuation while affecting the roll-off of the filters. By showing that less cells cause less attenuation, the attenuation could be

associated with an impedance mismatch due to two possible reasons. The first reason was for the impedance mismatch from overetching of the transmission line. The second reason was for the impedance mismatch associated with a finite ground plane with missing ground plane from the CSRR rings. Figures 5.11 through 5.16 show two separate filters with both orientations on one pvc pipe along with one set of calibration data to compare.

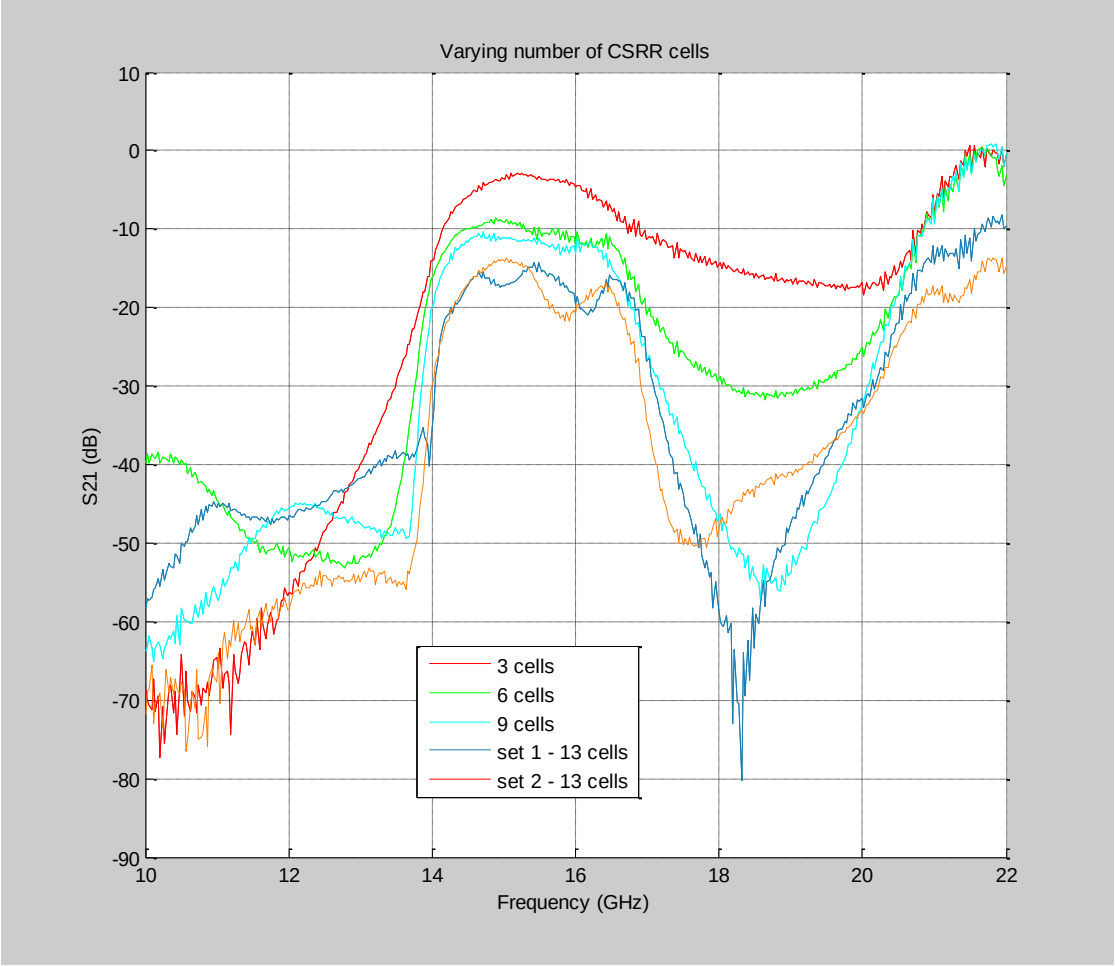

Figure 5.10: Various length CSRR arrays

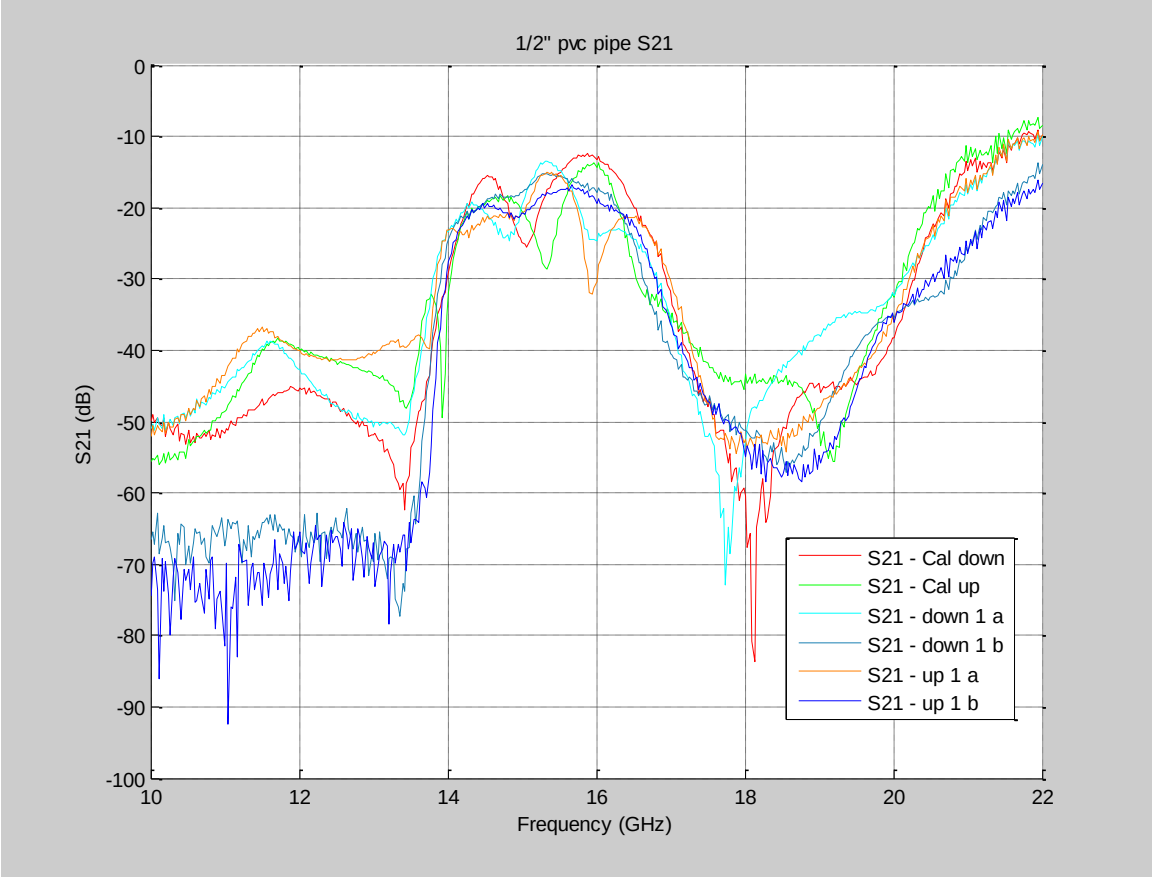

Figure 5.11: ½” pvc pipe S21

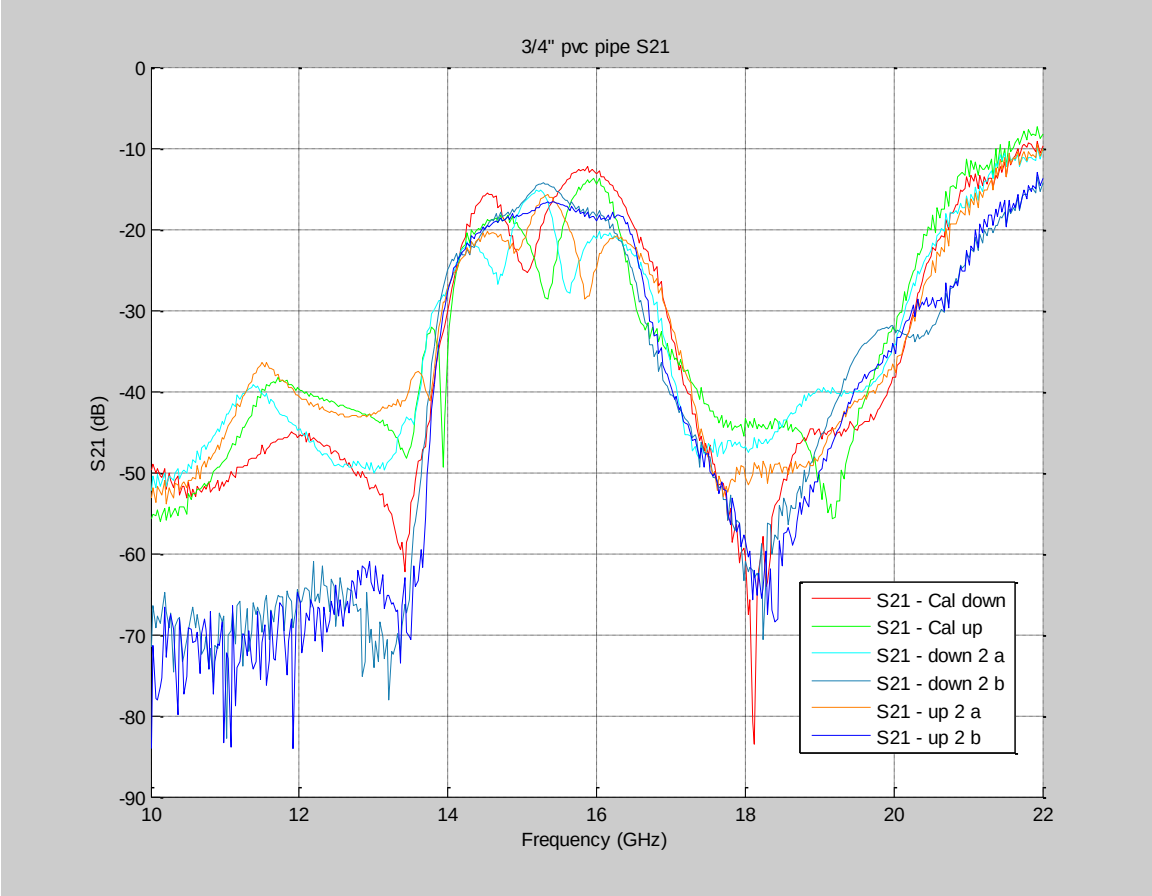

Figure 5.12: ¾” pvc pipe S21

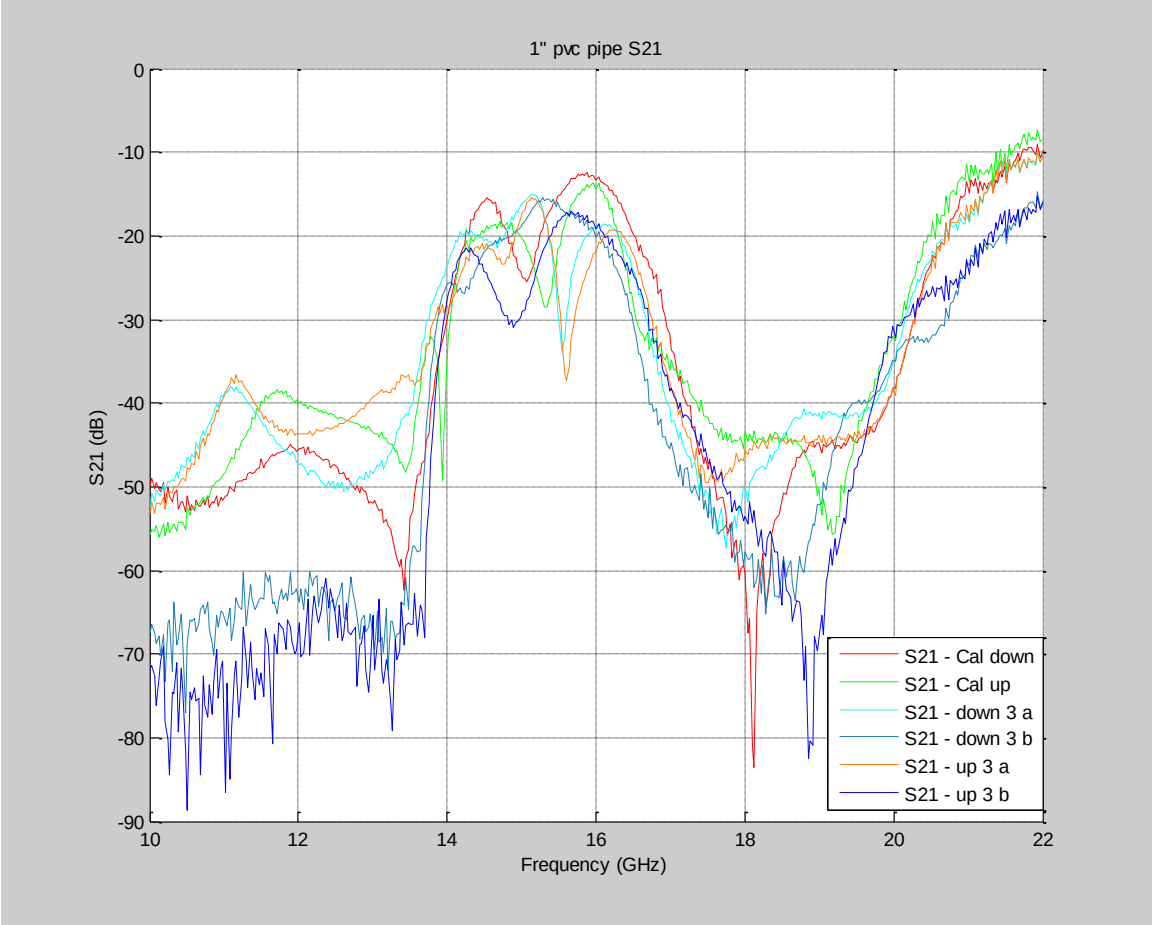

Figure 5.13: 1” pvc pipe S21

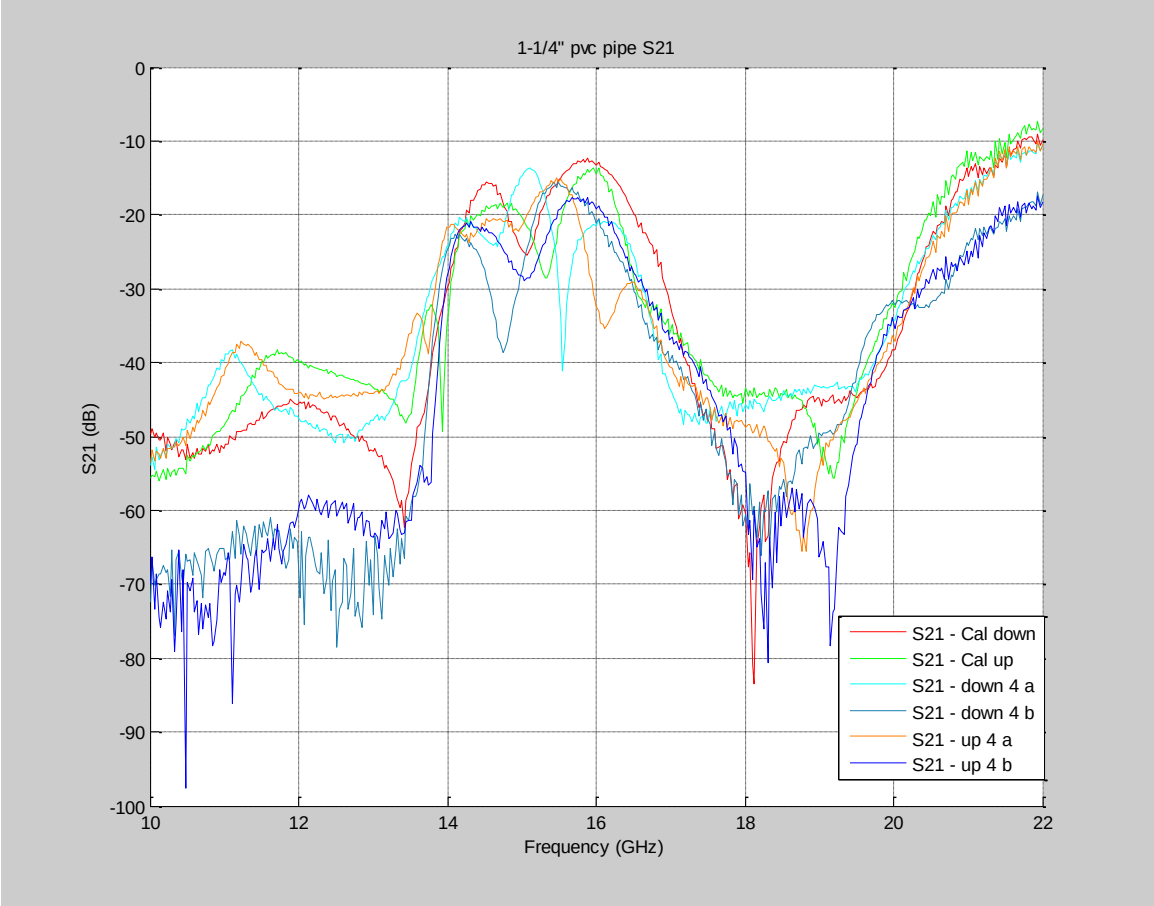

Figure 5.14: 1- ¼” pvc pipe S21

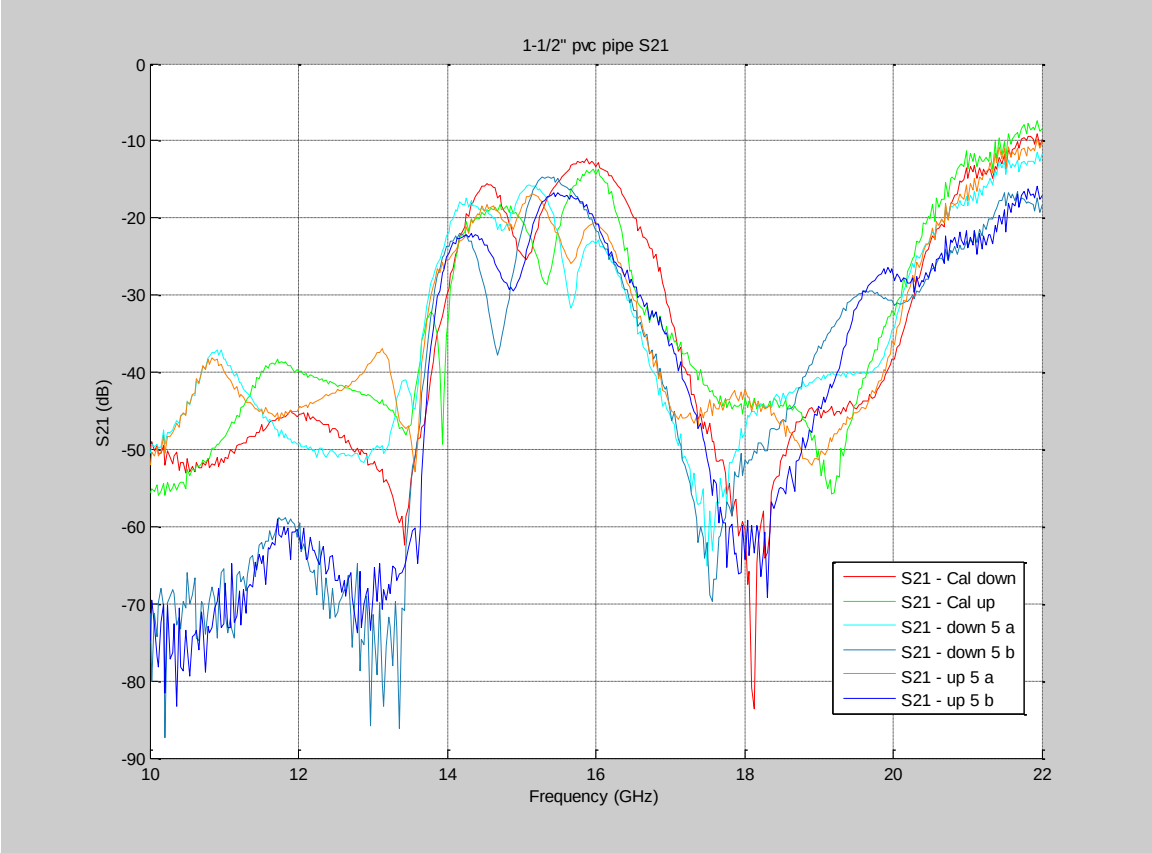

Figure 5.15: 1- ½” pvc pipe S21

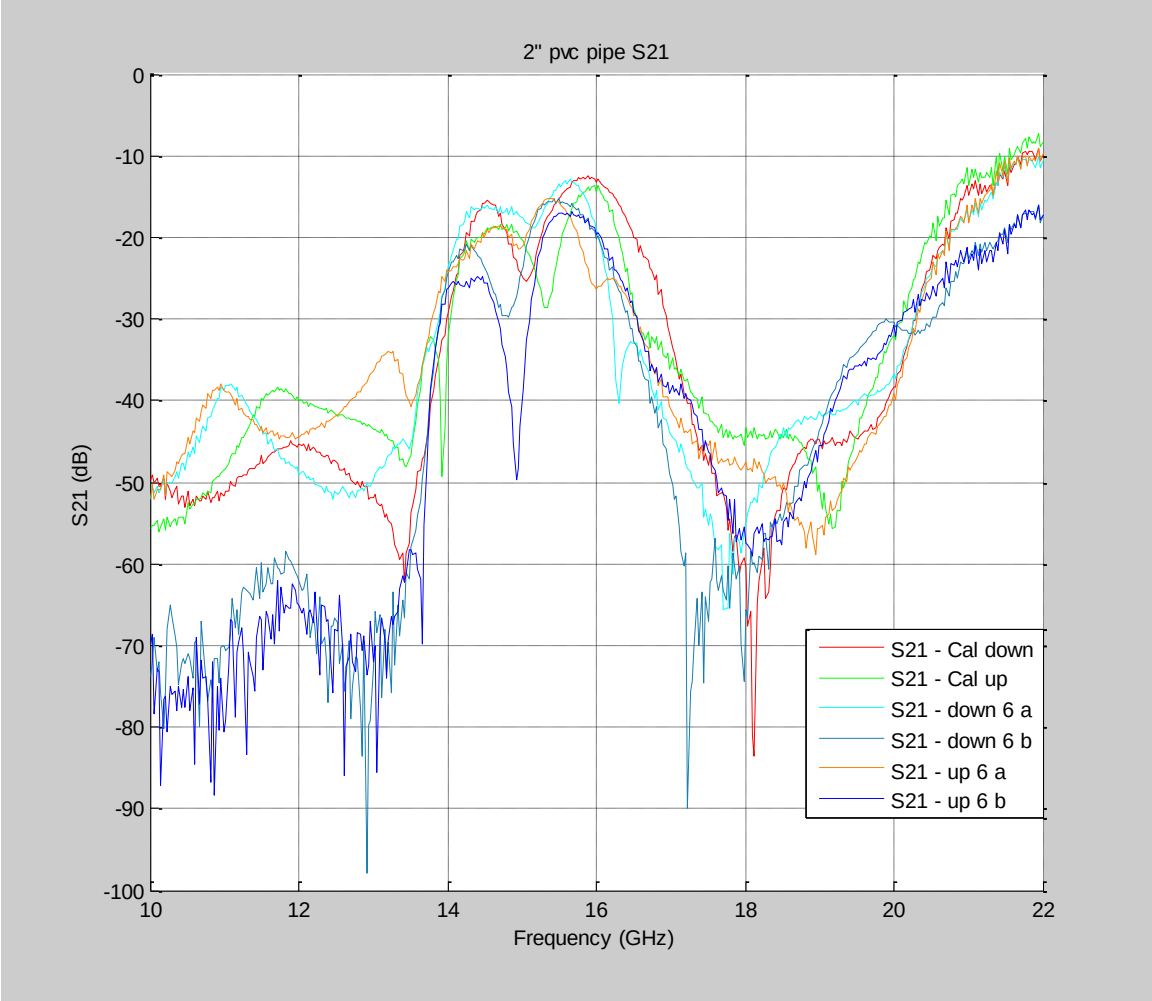

Figure 5.16: 2 ” pvc pipe S21

6. Conclusion

LCP has been shown to be a viable substrate to build metamaterial structures. Simulations of the structures were designed in ADS. The layouts were then made in ViewMaster. Then the use of MEMS fabrication processes such as photolithography were used in order to develop the metamaterial structures on LCP. Next, a test setup was built in order to test the filters while being flexed. Then the filter properties were shown to maintain approximately the same frequency and roll-off while being bent over various radii of curvature.

7. Future Work

There are numerous potential avenues to pursue for future work. One possibility will involve developing a 3-D invisibility cloak. Another possibility will be to deposit a layer of non-conductive substrate such as polyimide onto the existing structures.

In order to develop a 3-D cloak, a three dimensional layout must be simulated first. Proper 3-D modeling software would have to be selected for simulation. Once simulated, the mask layout could be designed and the structures could be built on LCP with the previously used photolithography process. Then the sheet of CSRR structures could be tested in an RF anechoic chamber.

Another future work would be to add polyimide to the existing structures. By adding a layer of polyimide on top of the LCP, the feature sizes could effectively be shrunk or bandwidth increased while maintaining similar operating frequencies. This is because the material deposited on the substrate would be of much higher dielectric constant than air. The capacitance across the gap would benefit from deposition of the material by effectively increasing proportional to the dielectric constant. A side benefit to having the layer of polyimide would be that any object that comes in contact with the polyimide would affect the filters significantly less than without any polyimide.

References

[1] Gil, M.; Bonache, J.; Selga, J.; Garcia-Garcia, J.; Martin, F., "Broadband Resonant-Type Metamaterial Transmission Lines," Microwave and Wireless Components Letters, IEEE , vol.17, no.2, pp.97-99, Feb. 2007

[2] Baena, J.D.; Bonache, J.; Martin, F.; Sillero, R.M.; Falcone, F.; Lopetegi, T.; Laso, M.A.G.; Garcia-Garcia, J.; Gil, I.; Portillo, M.F.; Sorolla, M.; , "Equivalent-circuit models for split-ring resonators and complementary split-ring resonators coupled to planar transmission lines," Microwave Theory and Techniques, IEEE Transactions on , vol.53, no.4, pp. 1451- 1461, April 2005

[3] Li C., Liu K. Y., Li F., "A microstrip highpass filter with complementary split ring resonators" PIERS Online, Vol. 3, pp 583-586, 2007, November 2007

[4] R. Dean, J. Weller, M. Bozack, C. Rodekohr, B. Farrell, L. Jauniskis, J. Ting, D. Edell and J. Hetke, "Realization of ultra fine pitch traces on LCP substrates," IEEE Trans. on Components and Packaging Technologies, Vol. 31, No. 2, pp. 315-321, June 2008

[5] X. Wang, J. Engel and C. Liu, "Liquid Crystal Polymer (LCP) for MEMS: Processes and Applications," J. Micromechanics and Microengineering, vol. 13, 2003, pp.628-633.

[6] Marque, Ricardo, Martin, F., and Sorolla, Mario, "Metamaterials with Negative Parameters: Theory, Design, and Microwave Applications" John Wiley and Sons Inc Publication, 2007

[7] Gil, M.; Bonache, J.; Gil, I.; Garcia-Garcia, J.; Martin, F, "On the transmission properties of left-handed microstrip lines implemented by complementary split ring resonators", International J of Numerical Modelling, Vol. 19, Issue 2, pp. 87-103, April 2006

[8] Hu Tao, N. I. Landy, Kebin Fan, A. C. Strikwerda, W. J. Padilla, R. D. Averitt, and Xin Zhang, "Flexible Terahertz Metamaterials: Towards a Terahertz Metamaterial Invisible Cloak" IEDM 2008 IEEE International, Dec 2008.

[9] Abul K. Azad, Hou-Tong Chen, Xinchao Lu, Jianqiang Gu, Nina R., Weisse-Bernstein, Elshan Akhadov, Antoinette J. Taylor, Weili Zhang, and John F.O'Hara, "Flexible Quasi-Three-Dimensional Terahertz Electric Metamaterials" Terahertz Science and Technology, Vol. 2, No. 1, March 2009

[10] Mingda Huang, M. Imran Kazim, Matti H. A. J. Herben, "Characterization of the Relative Permittivity and Homegeneity of Liquic Crystal Polymer (LCP) in the 60 GHz Band", European Cooperation in the Field of Scientific and Technical Research, Nov. 2010

[11] Ari Sihvola, Metamaterials in electromagnetics, Metamaterials, Volume 1, Issue 1, March 2007, Pages 2-11, ISSN 1873-1988

[12] Vladimir M. Shalaev, Wenshan Cai, Uday K. Chettiar, Hsiao-Kuan Yuan, Andrey K. Sarychev, Vladimir P. Drachev, and Alexander V. Kildishev, "Negative index of refraction in optical metamaterials", Optics Letters, Vol. 30, Issue 24, pp. 3356-3358 (2005)

[13] Jason Valentine1,3, Shuang Zhang1,3, Thomas Zentgraf1,3, Erick Ulin-Avila1, Dentcho A. Genov1, Guy Bartal1 & Xiang Zhang, "Three-dimensional optical metamaterial with a negative refractive index", Nature 455, 376-379, September 2008

[14] Andrea Alù and Nader Engheta, "Three-dimensional nanotransmission lines at optical frequencies: A recipe for broadband negative-refraction optical metamaterials", Phys. Rev. B 75, 024304 (2007)

[15] D. Schurig1, J. J. Mock, B. J. Justice, S. A. Cummer, J. B. Pendry, A. F. Starr and D. R. Smith, "Metamaterial Electromagnetic Cloak at Microwave Frquencies", Science 10 November 2006: Vol. 314 no. 5801 pp. 977-980

[16] Andrea Alù and Nader Engheta, "Multifrequency Optical Invisibility Cloak with Layered Plasmonic Shells", Phys. Rev. Lett. 100, 113901 (2008)

[17] Ricardo Marqués, Francisco Mesa, Jesús Martel, and Francisco Medina, "Comparative Analysis of Edge- and Broadside-Coupled Split Ring Resonators for Metamaterial Design – Theory and Experiments", IEEE Transactions on Antennas and Propagation, Vol. 51, No. 10, October 2003

[18] http://whites.sdsmt.edu/classes/ee481/mom.pdf

[19] Varadan, V.V.; , "Radar Absorbing Applications of Metamaterials," Region 5 Technical Conference, 2007 IEEE , vol., no., pp.105-108, 20-22 April 2007

[20] Pekka Alitalo and Sergei Tretyakov, “Electromagnetic cloaking with metamaterials,” Vol. 12, Issue 3, March 2009, pp 22-29

[21] http://www.rogerscorp.com/acm/index.aspx

[22] Kapitanova, P.; Kholodnyak, D.; Humbla, S.; Perrone, R.; Mueller, J.; Hein, M.A.; Vendik, I.B.; , "Multi-band and tunable multi-band microwave resonators and filters based on cascaded left/right-handed transmission line sections," *EUROCON 2009, EUROCON '09. IEEE* , vol., no., pp.39-45, 18-23 May 2009

[23] Gil, M.; Bonache, J.; Selga, J.; Garcia-Garcia, J.; Martin, F.; , "Broadband Resonant-Type Metamaterial Transmission Lines," *Microwave and Wireless Components Letters, IEEE* , vol.17, no.2, pp.97-99, Feb. 2007

[24] Bonache, J.; Gil, M.; Gil, I.; Garcia-Garcia, J.; Martin, F.; , "On the electrical characteristics of complementary metamaterial resonators," *Microwave and Wireless Components Letters, IEEE* , vol.16, no.10, pp.543-545, Oct. 2006

[25] Bonache, J., F. Martin, et al., “Application of complementary split-ring resonators to the design of compact narrow band-pass structures in microstrip technology,” Microw. and Opt. Techn.

[26] Ari Sihvola, Metamaterials in electromagnetics, Metamaterials, Volume 1, Issue 1, March 2007, Pages 2-11, ISSN 1873-1988

[27] Ricci, M.C.; Hua Xu; Prozorov, R.; Zhuravel, A.P.; Ustinov, A.V.; Anlage, S.M.; , "Tunability of Superconducting Metamaterials," *Applied Superconductivity, IEEE Transactions on* , vol.17, no.2, pp.918-921, June 2007

[28] Xuefeng Wang, Jonathan Engel and Chang Liu, “Liquid crystal polymer (LCP) for MEMS: processes and applications,” Journal of Micromechanics and Microengineering, Vol. 13, No. 5, 2003

[29] Islam, R.; Elek, F.; Eleftheriades, G.V.; , "Coupled-line metamaterial coupler having co-directional phase but contra-directional power flow," *Electronics Letters* , vol.40, no.5, pp. 315- 317, 4 March 2004

[30] Rohat Melik, Emre Unal, Nihan Kosku Perkgoz, Christian Puttlitz, and Hilmi Volkan Demir, “Flexible metamaterials for wireless strain sensing,” Appl. Phys. Lett. 95, Vol 95., Issue 18, Nov. 4, 2009

[31] Alitalo, P.; Luukkonen, O.; Jylha, L.; Venermo, J.; Tretyakov, S.A.; , "Transmission-Line Networks Cloaking Objects From Electromagnetic Fields,"

Antennas and Propagation, IEEE Transactions on , vol.56, no.2, pp.416-424, Feb. 2008

[32] Cheng-Jung Lee; Leong, K.M.K.H.; Itoh, T.; , "Metamaterial Transmission Line Based Bandstop and Bandpass Filter Designs Using Broadband Phase Cancellation," *Microwave Symposium Digest, 2006. IEEE MTT-S International* , vol., no., pp.935-938, 11-16 June 2006

[33] Antoniades, M.A.; Eleftheriades, G.V.; , "A broadband series power divider using zero-degree metamaterial phase-shifting lines," *Microwave and Wireless Components Letters, IEEE* , vol.15, no.11, pp. 808- 810, Nov. 2005

[34] Hu Tao, A.C. Strikwerda, K. Fan, C.M. Bingham, W. J. Padilla, Xin Zhang, and R. D. Averitt, "Terahertz metamaterials on free-standing highly-flexible polyimide substrates," Journal of Physics D: Applied physics, Vol. 41, No. 23, Dec. 13, 2008

[35] Clara Y. O. Lin and Joseph P. Curilla, "Temperature-Related Changes in Dielectric Constant and Dissipation Factor of Insulations Increase Attenuation in Data Cables Used in Building Plenums," IEEE, 1991

Microfabrication Process

1) Clean wafer with 10 mL HCl and 200 mL H20 for 60 seconds
2) Dehydrate wafer at 120 °C for 20 minutes
3) HMDS for 10 minutes
4) Spin on PR (photoresist) at 3000 rpm, 800 rev/s, for 30s using 8 mL AZ 4620
5) Softbake wafer at 105 °C for 60 to 90 seconds
6) Expose wafer for 14 seconds using multiple exposure 2 times
7) Develop the mask using 200 mL H20 and 100 mL AZ400 developer for 2 minutes
8) Place SAW tape onto non-developed side of wafer
9) Etch copper
10) Expose SAW tape to UV light for 20 seconds and remove tape
11) Dehydrate wafer at 120 °C for 20 minutes
12) HMDS for 10 minutes
13) Spin on PR at 3000 rpm, 800 rev/s, for 30s using 8 mL AZ 4620
14) Softbake wafer at 105 °C for 60 to 90 seconds
15) Expose wafer for 14 seconds using multiple exposure 2 times (use back side alignment (BSA) before exposure)
16) Develop the mask using 200 mL H20 and 100 mL AZ400 developer for 2 minutes
17) Place SAW tape onto non-developed side of wafer
18) Etch copper
19) Expose SAW tape to UV light for 20 seconds and remove tape
20) Remove PR from wafer by rinsing with acetone followed by alcohol and water

Bloch Impedance

Calculating Bloch Impedance:

```
%% constants
Cg = .69e-12;
C = 34.38e-12;
Lc = .036e-9;
Cc = 78.15e-12;
freq = 1e8:1e7:5e9;
w = 2*pi.*freq;

%% equations
Zb = sqrt( Lc./(Cc.*Cg.*w.*(1./(Cc.*w)-Lc.*w)) - 1./(4*Cg^2.*w.^2) -
1./(C*Cg.*w.^2) );
Zb2 = sqrt(Zb.^2);

%% plots
plot(freq./10^9,Zb2);
xlabel('Frequency (GHz)')
ylabel('Impedance (Ohms)')
```